Advances
in
Science
and
Technology
in
the USSR

Physics
Series

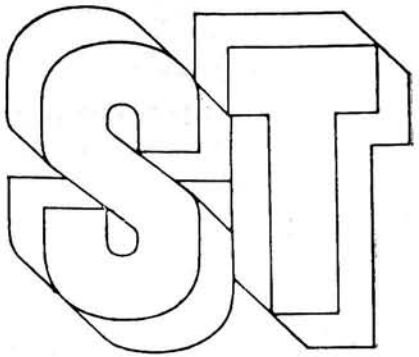

Problems in Solid-state Physics

Edited by A. M. PROKHOROV
Mem. USSR Acad. Sci.
A. S. PROKHOROV
Cand. Sc. (Phys. and Math.)

Translated from the Russian by
Ram S. Wadhwa, Ph. D.

Mir Publishers
Moscow

Проблемы физики твёрдого тела
Под редакцией акад. А. М. Прохорова
И канд. физ.-мат. наук А. С. Прохорова
Издательство «Мир» Москва

First published 1984

На английском языке

CONTENTS

3.63. I. E. Chupis and N. Ya. Aleksandrova, *Ukr. Fiz. Zh.*, **27**, 300 (1982).
3.64. I. A. Akhiezer and L. N. Davydov, *Ukr. Fiz. Zh.*, **15**, 1747 (1970); *Pis'ma v Zh. Eksp. Teor. Fiz.*, **13**, 380 (1971).
3.65. I. E. Chupis and V. N. Savchenko, in: *Some Questions in the Physics of Thin Ferromagnetic Films*, Vladivostok, 1974 (in Russian), p. 93.
3.66. I. A. Akhiezer and L. N. Davydov, *Fiz. Tverd. Tela*, **13**, 1795 (1971).
3.67. V. A. Nikitov, *Trudy MFTI, Ser. Radiotekhnika i Elektronika*, No. 9, 118 (1975).
3.68. A. S. Bakay and I. E. Chupis, *Fiz. Nizkikh Temp.*, **3**, 1153 (1977).
3.69. A. I. Akhiezer, V. G. Baryakhtar, and S. V. Peletminskii, *Spin Waves*, Nauka, Moscow, 1967 (in Russian), Sec. 14.
3.70. E. Ascher, H. Rieder, H. Schmid, and H. Stössel, *J. Appl. Phys.*, **37** 1404 (1966).
3.71. O. V. Kovalev, *Fiz. Tverd. Tela*, **14**, 307 (1972).
3.72. I. E. Chupis, *Fiz. Nizkikh Temp.*, 9, 56 (1983).
3.73. H. Schmid, in: *Crystal Growth*, Nauka, Moscow, 1967 (in Russian), Vol. 7, p. 32.
3.74. M. Tadashi and M. Tashiaki, *J. Phys. Soc. Japan*, **29**, 1092 (1970).
3.75. L. N. Baturov, R. V. Zorin, B. I. Al'shin, and Yu.N.Yarmukhamedov, *Fiz. Tverd. Tela*, **22**, 279 (1980).
3.76. A. V. Kovalev and G. T. Andreeva, *Fiz. Tverd. Tela*, **21**, 1744 (1979).
3.77. L. N. Baturov, B. I. Al'shin, and Yu.N. Yarmukhamedov, *Fiz. Tverd. Tela*, **20**, 2254 (1978).
3.78. L. N. Baturov and B. I. Al'shin, *Fiz. Tverd. Tela*, **21**, 3 (1979).
3.79. J. P. Rivera and H. Schmid, *Ferroelectrics*, **36**, 447 (1981).
3.80. J. P. Rivera, H. Schmid, J. M. Moret, and H. Bill, *Intern. J. Magnet.*, **6**, 211 (1974).
3.81. H. Minetaka, K. Kay, and K. Jinzo, *J. Phys. Soc. Japan*, **39**, 1625 (1975).
3.82. L. N. Baturov, B. I. Al'shin, and R. V. Zorin, in: *Abstracts of Papers to the All-Union Conf. on Magnetic Phenomena Physics*, Kharkov, 1979, p. 165.
3.83. G. T. Rado and J. M. Ferrari, *Phys. Rev. B. Solid State*, **15**, 290 (1977).
3.84. D. N. Astrov, B. I. Al'shin, R. V. Zorin, and L. A. Drobyshev, *Zh. Eksp. Teor. Fiz.*, **55**, 2122 (1968).
3.85. B. I. Al'shin, D. N. Astrov, and L. N. Baturov, *Pis'ma v Zh. Eksp. Teor. Fiz.*, **22**, 444 (1975).
3.86. L. N. Baturov, B. I. Al'shin, and D. N. Astrov, *Fiz. Tverd. Tela*, **19**, 916 (1977).
3.87. L. N. Baturov, R. V. Zorin, B. I. Al'shin, and V. I. Bugakov, *Fiz. Tverd. Tela*, **23**, 908 (1981).
3.88. N. N. Krainik, N. P. Khuchua, and V. V. Zhdanova, in: *Proc. of Intern. Meeting of Ferroelectrics*, Prague, 1966, V. 1, p. 377.
3.89. Yu. E. Roginskaya, Yu. Ya. Tomashpol'skii, Yu.N. Venevtsov, V. M. Petrov, and G. S. Zhdanov, *Zh. Eksp. Teor. Fiz.*, **50**, 69 (1966).
3.90. S. N. Drozhdin, B. G. Bochkov, N. D. Gavrilova, T. V. Popova, V. A. Koptsik, and V. K. Novik, *Kristallografiya*, **20**, 854 (1975).
3.91. G. A. Samara and P. M. Richards, *Phys. Rev. Ser. B*, **14**, 5073 (1976).
3.92. G. A. Samara and I. F. Scott, *Solid State Comm.*, **21**, 167 (1977).
3.93. D. L. Fox, D. R. Tilley, I. F. Scott, and H. I. Guggenheim, *Phys. Rev. Ser. B*, 21, 2926 (1980).
3.94. D. E. Cox, S. M. Shapiro, R. A. Cowley, I. M. Eibschütz, and M. I. Guggenheim, *Phys. Rev. Ser. B*, **19**, 5754 (1979).
3.95. J. H. Brunskill and H. Schmid, *Ferroelectrics*, **36**, 395 (1981).
3.96. I. H. Ismailzade and R.Y.Yakupov, *Phys. Stat. Sol., Ser.(a)*, **32**, K161 (1975).
3.97. I. Van den Boomgaard and R.A.I.A. Born, *J. Mater. Sci.*, **13**, 1538 (1978).
3.98. E. Wood and A. E. Austin, *Intern. J. Magnet.*, **5**, 303 (1974).
3.99. K. Leibler, V. A. Isupov, and H. Bielska-Landowska, *Acta Phys. Polon., Ser. A*, **40**, 815 (1971).

4 High Hydrogen Pressures. Synthesis and Properties of New Hydrides

E. G. Ponyatovsky, V. E. Antonov, and I. T. Belash

4.1. INTRODUCTION

For many years, the properties of transition metal-hydrogen systems have drawn the attention of researchers working in diverse fields of physics and material science. There are several reasons for the growing interest in the problem "hydrogen in metals". These include the unusual physical properties of metal-hydrogen systems caused by the unique nature of hydrogen as a component, the profound effect of hydrogen on mechanical, physical, and chemical properties even at extremely low concentrations, and a wider range of practical applications of metal-hydrogen systems (purification and accumulation of hydrogen, separation of its isotopes, designing new types of heat exchangers, catalyzers, and so on). The intensive studies on the interaction of hydrogen with metals were largely stimulated by investigations in the field of hydrogen power engineering and thermonuclear fusion. The possibility of using hydrogen as a universal power source has shed a new light on the question of developing structural materials that are stable to hydrogen. The construction of apparatus using plasma requires a knowledge of the peculiarities of the interaction of reactor materials with hydrogen in the state of enhanced thermodynamic activity.

In spite of the extensive investigations that have been conducted throughout the world to study the metal-hydrogen systems, the data on the physical properties of solutions of hydrogen even in such important and interesting transition metals as Fe, Co, Ni, Cr, Mn, and Mo has remained scarce so far. As a matter of fact, the solubility of hydrogen in these metals is extremely low at atmospheric pressures, and a huge amount of experimental data concerning the influence of hydrogen on the properties of these metals and their alloys was obtained for hydrogen concentrations usually not exceeding the H-to-metal atomic ratio $n \approx 10^{-5}$-10^{-7}. Such concentrations are comparable with those of various defects (hydrogen traps), and this complicates the physical interpretation of the accumulated experimental data.

In order to isolate the role of hydrogen as an alloying element in forming physical properties of a system under consideration and to analyze the important question about the physical status of hydrogen

in transition metals, we must be able to freely vary the hydrogen content over a wide interval. This may be accomplished by varying the chemical potential of hydrogen. An increase in the chemical potential of hydrogen shifts the thermodynamic equilibrium in the metal-excess hydrogen systems towards higher concentrations of Me-H solid solutions right up to the formation of hydrides of stoichiometric compositions. For example, it was observed in [4.1] that the interaction of hydrogen plasma with molybdenum leads to the formation of hydrogen-saturated phases with compositions up to MoH_2.

Earlier, the increase in the hydrogen content of transition metals was mainly attained by electrochemical methods which were first used to obtain hydrides of nickel and chromium. Later, hydrogen implantation and diverse methods of plasma synthesis were used for this purpose. However, the use of these methods imposes severe limitations on the geometrical dimensions and the quality of the samples obtained. In the case of electrochemical saturation and implantation, the samples are usually thin films of a few microns thickness, while for plasma synthesis we obtain fine powders with numerous defects. The high density of defects in hydrogenated films and powders may be the reason behind specific physical properties which are not inherent in the bulk samples of the same composition. By way of an example, we refer the reader to communication [4.2] about the transition of thin palladium films to the superconducting state upon irradiation by alpha-particles.

4.2. METHODS FOR COMPRESSING HYDROGEN AND OBTAINING HYDRIDES

All these drawbacks can be directly eliminated if hydrides are synthesized by placing the metal in an atmosphere of hydrogen whose thermodynamic potential is raised by compression to high pressures. The work with high-pressure gases, however, involves many experimental difficulties, and even for inert gases the upper limit of pressures attainable with the help of more or less assimilated techniques does not exceed 2-3 GPa. These difficulties are considerably enhanced in the case of hydrogen due to its high compressibility, extremely low viscosity, and chemical corrosiveness which greatly increases with temperature and pressure. For this reason, until the last decade, the investigation of metal-hydrogen systems was restricted to pneumatic pressures (10-15 MPa) and in individual cases to a few hundred MPa. This range of pressures was first exceeded in the middle of 1960s by Polish scientists who designed a system in which a bronze bomb containing hydrogen was placed in a hydrostatic high-pressure chamber [4.3]. This made it possible to isolate the chamber walls from the direct influence of hydrogen and to use

steel chambers for compressing hydrogen up to $P_{H_2} \approx 2.5$-3 GPa at room temperature and to $P_{H_2} \approx 1.5$ GPa at $T \leqslant 450$°C.

The significant increase in the pressure and temperature range permitted synthesizing nickel- and chromium hydrides under equilibrium conditions and obtaining for the first time manganese hydride and hydrogen-saturated phases based on a series of nickel and palladium alloys, as well as studying their crystal structure and thermal stability, and investigating of their magnetic and superconducting properties (a detailed review of research conducted during this period is given in [4.4-6]).

The abilities of "piston-cylinder" type hydrostatic chambers are practically exhausted by pressures of the order of 3 GPa. By using the method proposed in [4.7] for obtaining high hydrogen pressures, we were able to overcome this barrier. The method consists in the following. A condensed hydrogen-containing compound is introduced into an ampoule-type container. The container is placed into a high-pressure chamber, preliminary compression is performed, and hydrogen is freed by decomposing the compound by any known means. The temperature and pressure in the operating zone of the high-pressure chamber and, hence, of hydrogen in the container are then brought up to the required values. With the help of this method, a series of high pressure cells was created at the Institute of Solid State Physics of the USSR Academy of Sciences. This allowed an investigation of the behaviour of the Curie points and electrical resistance of specimens under hydrogen pressure from ~3 MPa to 9 GPa at $-150 \leqslant T \leqslant 500$°C.

Thermal decomposition is the simplest way to release hydrogen from a compound. The block diagram of cells for measuring the electrical resistance of samples in which this method is used is shown in Fig. 4.1. No external source is required for filling the ampoule with hydrogen, since hydrogen is released during thermally activated decomposition of the hydride (*03*, *14*) placed beforehand in the lower part of the ampoule. Elimination of the appropriate filling system from the scheme permits complete utilization of the potentialities of ordinary hydrostatic high-pressure chambers, while the appreciable simplification of the construction permits production of cells of quite small dimensions (Fig. 4.1, cell *11-17*) which can be placed into the operation zone of the existing quasihydrostatic chambers. It is the use of the quasihydrostatic chambers that made it possible to overcome the limit ~3 GPa and to compress hydrogen to 9 GPa. It should be noted that even this limit of 9 GPa is set by the chambers at our disposal and not by the method proposed in [4.7]. Readers interested in details of the application of this method are referred to the articles listed in [4.8].

By the middle of 1970s, there remained twelve transition elements in the Periodic Table for which hydrides were not obtained:

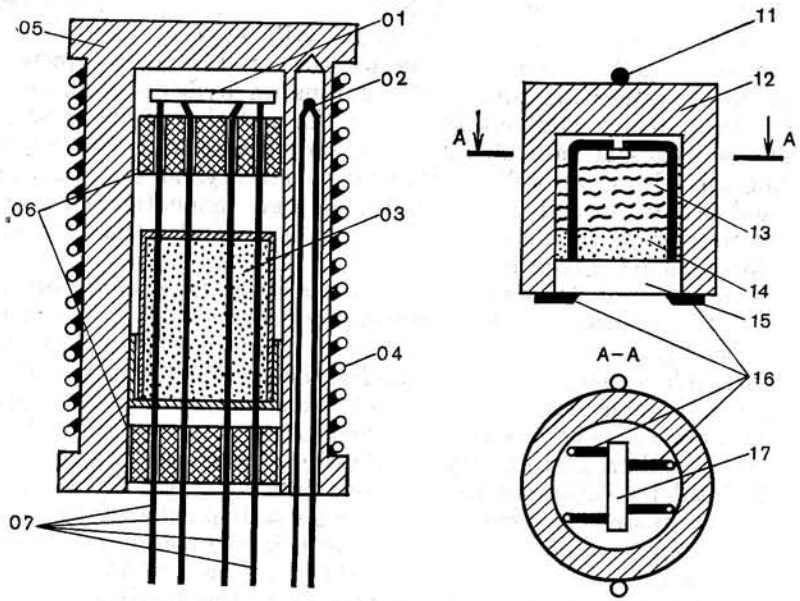

Fig. 4.1. Block diagram of cells for measuring the electrical resistance of samples in hydrogen atmosphere using hydrostatic (*01-07*) and quasi-hydrostatic (*11-17*) chambers.
01, *17*—sample; *02*, *11*—thermocouple junction; *03*, *14*—hydride (hydrogen source); *04*—heater; *05*—ampoule (brass); *06*—clamps (pyrophyllite); *07*, *16*—electrical leads; *12*—ampoule (Teflon); *13*—glass wool; *15*—ampoule cap (Teflon); all free space in the ampoules *05* and *12* is filled with silicone or petrol.

Mn, Fe, Co, Mo, Tc, Ru, Rh, W, Re, Os, Ir, and Pt. The application of the new method for compressing hydrogen reduced the number of such elements to six. We synthesized hydrides of manganese (simultaneously with Polish scientists), iron, cobalt, molybdenum, technetium, and rhodium. Significant quantities of hydrogen were introduced into Re and Ru. Gold hydride, the first member of the family of noble metal hydrides, was also synthesized by using the high-pressure technology [4.9].

The structure and limiting compositions of hydrogen solutions in group VI-VIII transition metals synthesized so far are shown in Table 4.1. All hydrides are formed only on the basis of one of the two closest packings of metal atoms, namely fcc (face-centred cubic, γ) or hcp (hexagonal close-packed, ε). It should be mentioned that here and subsequently we shall be dealing only with massive samples. Apparently, if the samples are in the form of thin films, hydrides with other compositions and structures can be formed. For example, it is reported in [4.10] that heating a 500-1000 Å thick film of palla-

Table 4.1. Hydrides of Transition Metals

VI	VII	VIII		
ε $CrH_{1.0}$	ε $MnH_{0.96}$	ε $FeH_{0.8}$	ε, γ $CoH_{1.0}$	γ $NiH_{1.25}$
ε $MoH_{1.3}$	ε $TcH_{0.83}$	ε $RuH_{0.03}$	γ $RhH_{1.0}$	γ $PdH_{1.0}$
W	ε $ReH_{0.22}$	Os	Ir	Pt

Remark: The maximum attained hydrogen concentration is indicated; ε are solutions with hcp metal lattice; γ are solutions with fcc metal lattice.

dium up to $T \gtrsim 600$°C in a hydrogen atmosphere at $P_{H_2} = 0.1$ MPa results in the formation of $PdH_{1.33}$ with a tetragonal lattice having the parameters $a = 2.896$ Å and $c = 3.330$ Å at room temperature (such a hydride was initially obtained by the same authors by implantation of hydrogen into palladium). A similar treatment of massive samples led to the formation of ordinary Pd-H solutions with fcc metal sublattices.

All the investigated hydrides of transition metals are characterized by a metallic conductivity of the order of the conductivity of the starting metal. The kinetics of hydrogen absorption (hydride formation) varies from metal to metal over an extremely wide interval: at $T = 250$°C, from several minutes for palladium [4.11, 12] and nickel [4.12, 13] to tens of hours for technetium [4.14] (the samples are foils of 0.1-0.2 mm thickness). A similar diversity is also observed in the kinetics of thermal decomposition of hydrides into metal and molecular hydrogen under atmospheric conditions: hydrides of manganese [4.15, 16] and technetium [4.17] are metastable at 20°C, while hydrides of iron [4.18] and rhodium [4.19] rapidly decompose at $T \approx -100$°C onwards. In liquid nitrogen, all hydrides without exception last indefinitely. Taking into account such kinetics of formation and decomposition of hydrides, systems for "quenching" the samples were developed. The sample is first saturated with hydrogen at high pressure and temperature. After this, the sample is rapidly cooled (down to —180°C, if necessary) without changing the pressure. The pressure is then brought down to the atmospheric level, and the sample is taken out of the chamber for

a subsequent study of its physical properties. The investigation of these metastable (relative to decomposition into metal and molecular hydrogen) hydrides under atmospheric pressure considerably supplemented the results of measurements under high hydrogen pressure.

In the following sections, we shall describe the results of investigation of phase diagrams of metal-hydrogen systems, crystal structure, thermal stability, as well as magnetic and superconducting properties of recently obtained hydrides.

4.3. PHASE TRANSFORMATIONS IN METAL-HYDROGEN SYSTEMS

Cr-H. Chromium can be electrolytically saturated with hydrogen to compositions close to CrH [4.20]. Depending on the conditions of electrolysis, hydrides thus obtained can either have an fcc or an hcp lattice of the metal.

Baranowski and Bojarski [4.21] were the first to synthesize chromium hydride through a direct interaction of the metal with hydrogen at high pressures. A noticeable solubility of hydrogen in bcc (body-centered cubic) chromium (α-phase) was not observed. Chromium hydride (ε-phase) is formed on the basis of an hcp lattice whose parameters at $T = -190$°C and under atmospheric pressure are $a = 2.717$ Å, $c = 4.436$ Å, and $c/a = 1.633$ [4.21]. Our measurements have shown that the composition of the hydride is close to the CrH stoichiometry over the entire investigated stability range on the T-P_{H_2} diagram right up to $T = 400$° C and $P_{H_2} = 7$ GPa.

The formation of chromium hydride is accompanied by a considerable (several tens per cent) increase in the sample resistance, the decomposition—by its decrease. Figure 4.2 shows the T-P_{H_2} phase diagram of the Cr-H system, constructed mainly on the basis of resistometric data [4.22]. It can be seen from the phase diagram that the considerable hysteresis in the $\alpha \rightleftarrows \varepsilon$ transformation persists at all temperatures right up to 400 °C. Apparently, this hysteresis is caused by the elastic stresses which are close to the yield stress and appear in the sample due to an abrupt increase in the volume ($\approx 19\%$) upon hydride formation. In this case, the curve of thermodynamic equilibrium between the α- and ε-phases must be much closer to the hydride decomposition curve than to the hydride formation curve, since the removal of even a small amount of hydrogen leads to a relaxation of the elastic stresses [4.4]. For the Cr-H system, such an assumption is confirmed by a satisfactory agreement between the calculated value of the thermodynamic equilibrium pressure at room temperature [4.23] and the experimental curve for the $\varepsilon \rightarrow \alpha$ transition (Fig. 4.2.).

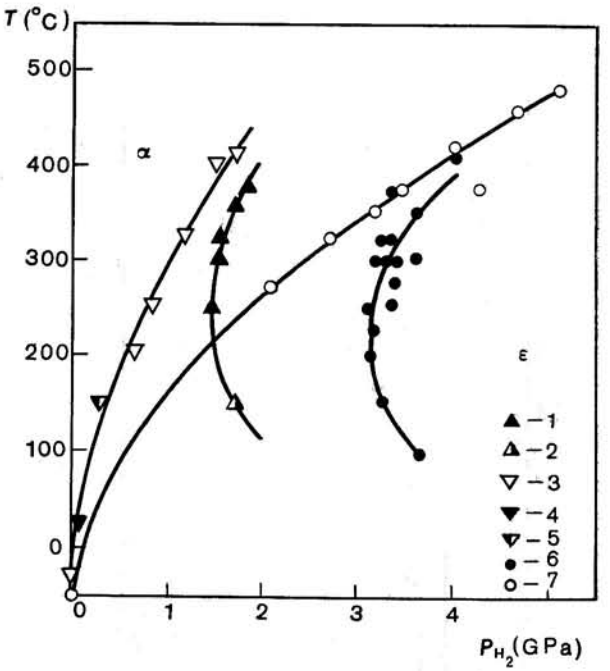

Fig. 4.2. T vs. P_{H_2} phase diagrams for the Cr-H (*1-5*) and Mo-H (*6, 7*) systems [4.25].
1, 6—pressure corresponding to $\alpha \rightarrow \varepsilon$ transitions; *3, 7*—pressure corresponding to $\varepsilon \rightarrow \alpha$ transitions; *2, 5*—results of [4.21] and [4.23]; *4*—calculated equilibrium pressure for $2Cr + H_2 \rightleftarrows 2CrH$ [4.23].

Mo-H. Molybdenum hydride was first synthesized under a high hydrogen pressure [4.24]. Figure 4.2 shows the T-P_{H_2} phase diagram of the Mo-H system, constructed on the basis of resistometric data [4.25]. Typical isotherms for the electrical resistivity of molybdenum in a hydrogen atmosphere, clearly indicating the jumps caused by the formation and decomposition of hydride, are shown in Fig. 4.3.

It can be seen from Fig. 4.2 that the T-P_{H_2} diagram for the Mo-H system is analogous to the diagram for the Cr-H system, and the curves corresponding to the formation and decomposition of molybdenum hydride are merely displaced towards the region of higher pressures. As in the case of bcc chromium, the solubility of hydrogen in bcc molybdenum is quite low. As to the ε-solutions, our recent measurements have shown that in the investigated stability region of molybdenum hydride on the T-P_{H_2} diagram (right up to $T = 400$° C and $P_{H_2} = 7$ GPa), its composition is close to $n \approx 1.2$-1.3 and de-

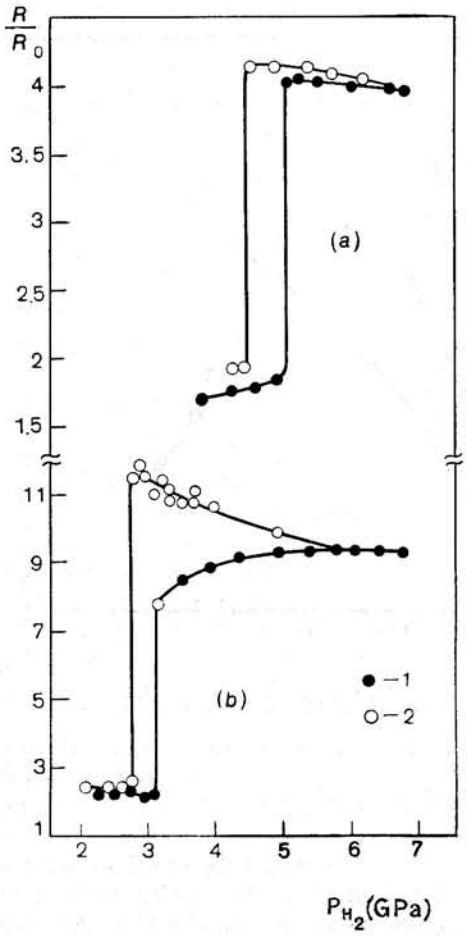

Fig. 4.3. Electrical resistivity isotherms for rhodium (*a*, $T = 300$°C) [4.47] and molybdenum (*b*, $T = 325$°C) [4.25] in hydrogen atmosphere.
1—with increasing pressure; *2*—with decreasing pressure. R_0 is the sample resistance at room temperature and under atmospheric pressure.

pends only slightly on the temperature and pressure of hydrogen. Under atmospheric pressure and at $T = -145$° C, the parameters of the hcp metallic sublattice of hydride are $a = 2.92$ Å, $c = 4.74$ Å, and $c/a = 1.63$ [4.24]. A transition of molybdenum hydride into superconducting state was not observed at $T \geqslant 2$ K.

W-H. No noticeable solubility of hydrogen in tungsten was observed at $T \leqslant 400$°C and $P_{H_2} \leqslant 9$ GPa.

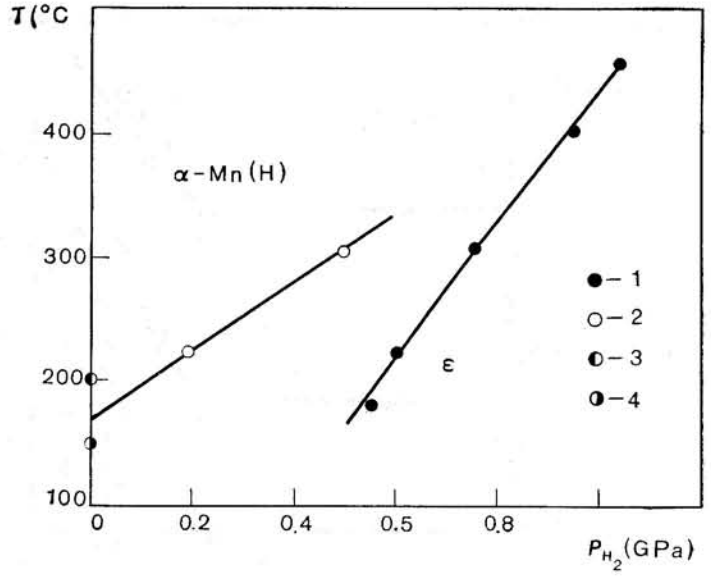

Fig. 4.4. T vs. P_{H_2} phase diagram for the Mn-H system.
1—points corresponding to the onset of hydride formation [4.26]; *2* [4.6], *3* [4.15], and *4* [4.16] are the points corresponding to the decomposition of the hydride.

Mn-H. Manganese hydride was first obtained under a high hydrogen pressure [4.15, 16]. The phase diagram of the Mn-H system is shown in Fig. 4.4. The values of pressures corresponding to the hydride formation have been obtained from the position of jumps in the electrical resistivity isotherms [4.26], while the pressures corresponding to its decomposition are determined from the hydrogen content in the Mn-H samples obtained by exposure to hydrogen atmosphere [4.6].

It can be seen from Fig. 4.4 that manganese hydride is stable under normal conditions. Figure 4.5 shows the dependence of the parameters of the hcp metallic lattice of manganese hydride on composition at room temperature [4.27]. A reduction in the hydrogen content of the samples to $n \approx 0.65$ leads to a monotonic decrease in the value of the parameters a and c of the hydride. In the concentration range $0 < n \leqslant 0.65$, where the parameters a and c remain practically unchanged, the samples consist of a mixture of the hydride and initial α-Mn. Thus, the region of existence of the continuous solid ε-solutions Mn-H (hydrides) at atmospheric pressure has a lower concentration limit $n_\varepsilon^{\min} \approx 0.65$ for which clear bends are observed in the *a*

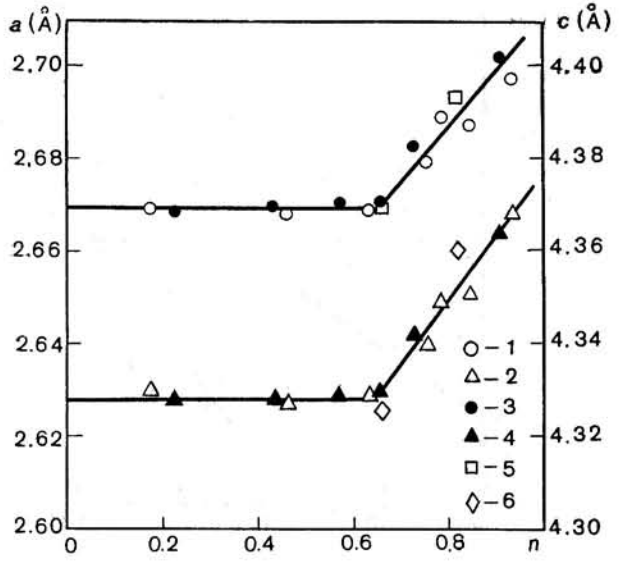

Fig. 4.5. Dependence of the parameters of the hcp metal lattice on n for Mn-H (light symbols) and Mn-D (dark symbols) solutions at room temperature [4.27].
1, *3*—parameter a; *2*, *4*—parameter c; *5*, *6*—results of [4.15].

vs. n and c *vs.* n curves. It is interesting to note (see Fig. 4.5) that the a (n) and c (n) dependences, as well as the value of $n_\varepsilon^{\min}$ for Mn-D solutions, are close to those for Mn-H solutions. Neutronographic studies of the deuteride $MnD_{0.65}$ at $T \geqslant 80$ K have shown [4.28] that deuterium atoms occupy the octahedral interstices in the hcp lattice of the metal.

Tc-H [4.17, 14]. In the investigated range of hydrogen pressures up to ~ 2.2 GPa, the Tc-H solutions are formed on the basis of the initial hcp lattice of the metal. The T-P_{H_2} diagram for the Tc-H system, however, turned out to be rather complicated: two isomorphic (at least so far as the metal lattice is concerned) phase transitions, $\varepsilon_0 \rightarrow \varepsilon_1$ and $\varepsilon_1 \rightarrow \varepsilon_2$, take place in the system and are accompanied by an abrupt increase in the solubility of hydrogen in technetium. It is interesting to note that in the hydrogen solubility isotherm for technetium at 300° C (Fig. 4.6), two regions of supercritical anomalies (near $P_{H_2} = 0.3$ and 1.3 GPa) are clearly seen for these transitions, terminating at the critical points at $T < 300°$ C.

The Tc-H solutions are kinetically stable under normal conditions. A rapid decomposition of the Tc-H hydrides takes place upon heating in vacuum to $T \geqslant 80°$ C. At room temperature and atmospheric

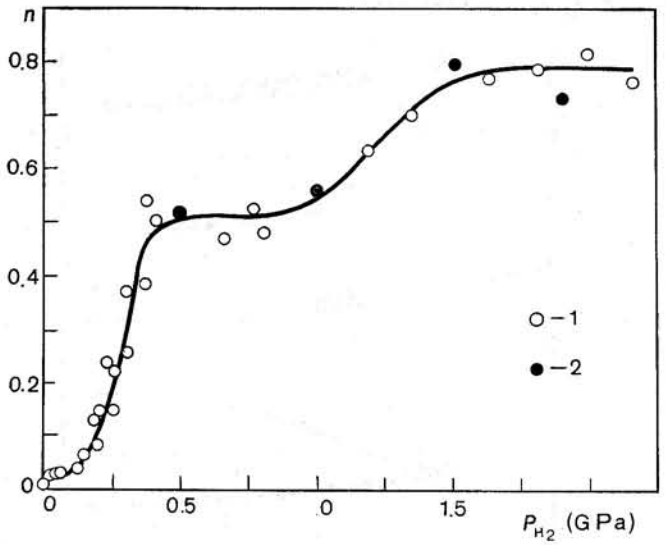

Fig. 4.6. Solubility of hydrogen in technetium at $T = 300$°C.
1—results of [4.14]; *2*—results of [4.17].

pressure, the maximum hydrogen solubility in the ε_0-phase amounts to $n \approx 0.04$; the samples with $0.04 \leqslant n \leqslant 0.39$ consist of a mixture of the ε_0-phase and ε-hydride, while from $n \approx 0.39$ to $n \approx 0.78$ the region of continous ε-solutions stretches[1]. Parameters of the metal lattice of the ε-hydride ($a = 2.805$ Å, $c = 4.455$ Å, and $c/a = 1.588$) remain unchanged, within experimental errors, for the entire concentration range $0.39 \leqslant n \leqslant 0.78$. The dissolution of hydrogen in the ε_0-phase decreases the superconducting transition temperature of technetium from $T_k = 7.85$ K for $n = 0$ to $T_k \approx 7.35$ K for $n \approx 0.04$. The Tc-H solutions in the ε-phase with $n \geqslant 0.39$ possess no superconductivity at $T \geqslant 2$ K.

Re-H [4.30]. At $T = 250°$ C, the solubility of hydrogen in rhenium increases monotonically with pressure, thus causing a smooth deviation of the pressure dependence of the electrical resistance of the

[1] It should be noted that the T-c diagram for the metastable equilibria in the Tc-H solutions under atmospheric pressure apparently differs considerably from the T-c projection of the equilibrium T-P_{H_2}-c diagram of the Tc-H system onto the plane $P_{H_2} \approx 0.1$ MPa. This difference is a quite common feature of Me-H systems (see [4.29]). In particular, this results in a need for reliable data on the phase composition of Me-H solutions for different values of external parameters, since only part of the investigations of physical properties of such solutions can be carried out directly at high hydrogen pressure, while other studies have to be conducted on samples in the metastable state.

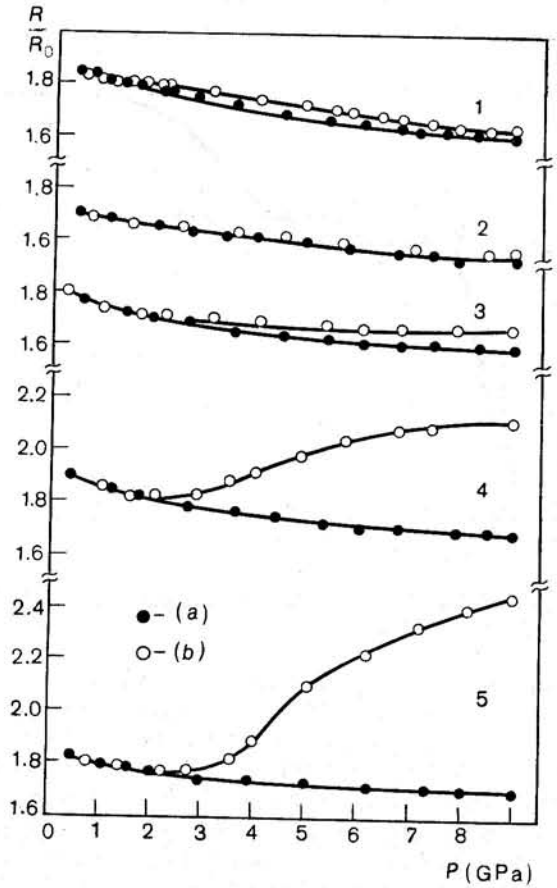

Fig. 4.7. Electrical resistance isotherms in an inert medium (*a*) and in hydrogen (*b*) at $T = 250$°C, obtained through a stepwise increase in pressure.
1—Pt; *2*—Ir; *3*—Os; *4*—Ru (results of the present paper); *5*—Re, results of [4.30]. R_0 is the same as in Fig. 4.3.

sample from the analogous dependence for rhenium in an inert atmosphere (Fig. 4.7). At this temperature and the pressure $P_{H_2} = 9$ GPa, the concentration of the Re-H solid solution attains the value $n = 0.13 \pm 0.03$. At $P_{H_2} = 9$ GPa, the equilibrium concentration of hydrogen in rhenium increases with decreasing temperature, reaching $n = 0.22 \pm 0.03$ at $T = 170$° C. Under atmospheric pressure, a noticeable evolution of hydrogen from Re-H samples begins at $T \gtrsim 0$° C.

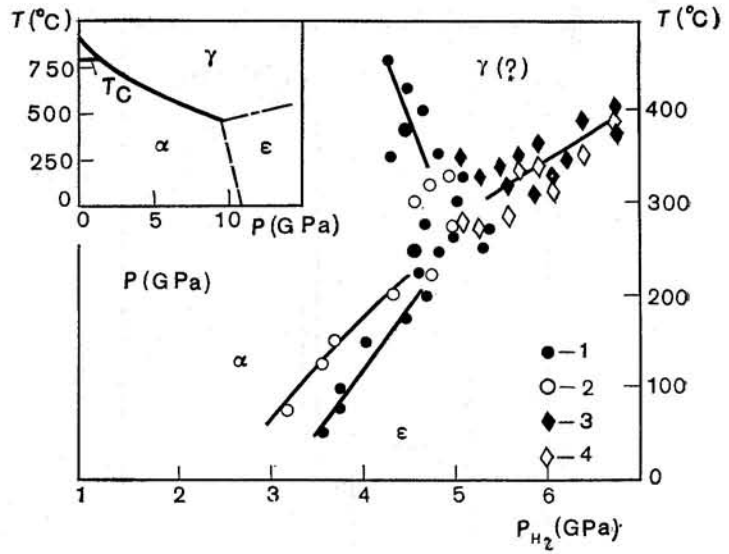

Fig. 4.8. T vs. P_{H_2} phase diagram for the Fe-H system [4.31]. *1*, *2*—position of anomalies on the electrical resistance isotherms (Fig. 4.9) for increasing and decreasing pressures respectively; *3*, *4*—position of anomalies on the electrical resistance isobars and initial magnetic susceptibility (Fig. 4.10) upon heating and colling respectively. The inset shows the T vs. P diagram for iron [4.32]; T_C is the line corresponding to Curie temperatures.

X-ray investigations at $T \approx -180$° C have shown that the introduction of hydrogen does not change the symmetry of the hcp lattice of rhenium, and leads only to a monotonic increase in the value of its parameters. The parameter a increases more rapidly than c, and the ratio c/a decreases from 1.615 for the initial rhenium to 1.591 for a sample with $n = 0.22$. The increase in V_a, the volume per rhenium atom, amounts to $\partial V_a/\partial n \approx 2.6$ Å^3 per H atom.

Dissolution of hydrogen causes a decrease in the value of T_k for Re from 1.87 K for $n = 0$ to 1.66 K for $n = 0.03 \pm 0.01$. For $n = 0.07 \pm 0.02$, the superconducting transition temperature falls to below 1.4 K.

Fe-H. Iron hydride was first synthesized at $P_{H_2} = 6.7$ GPa and $T = 250$° C [4.18]. The hydride had a composition $n \approx 0.8$. Under atmospheric pressure and $T \gtrsim -120$ °C, the hydride decomposed into the initial bcc iron and molecular hydrogen. According to X-ray investigations, iron hydride at $T = -190$° C has an hcp metal lattice with the parameters $a = 2.686$ Å, $c = 4.380$ Å, and $c/a = 1.631$.

Figure 4.8 shows the T-P_{H_2} diagram for the Fe-H system, wherein the locations of anomalies of temperature (Fig. 4.9) and baric (Fig.

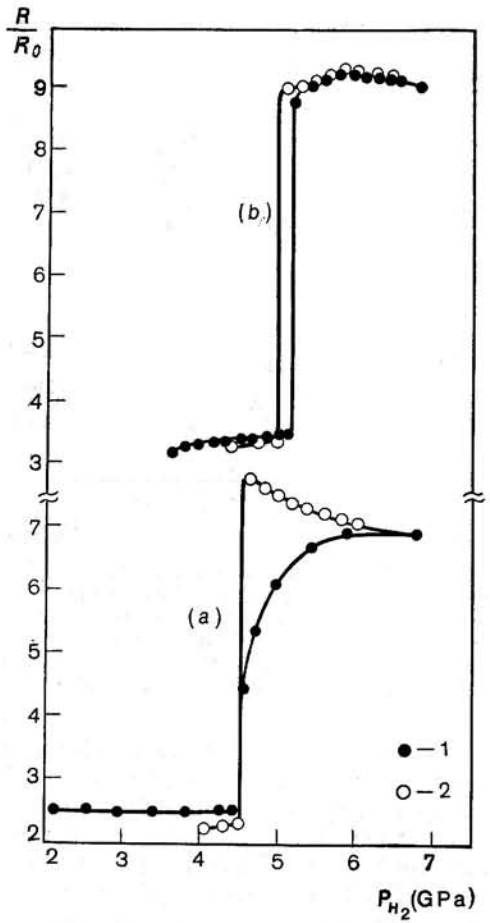

Fig. 4.9. Electrical resistance isotherms for iron in hydrogen atmosphere at $T = 250°C$ (*a*) and 330°C (*b*) [4.31].
1—with increasing pressure; *2*—with decreasing pressure. R_0 is the same as in Fig. 4.3.

4.10) dependences of electrical resistance of iron in a hydrogen atmosphere are indicated [4.31]. The lines of phase transformations divide the T-P_{H_2} plane of the diagram into three regions (α, ε, and γ), the coordinates of the triple point being $T \approx 280°$ C and $P_{H_2} \approx 5$ GPa. In the α-region, solutions having a bcc lattice for iron are thermodynamically stable (the concentration of these solutions does not exceed $n \approx 0.01$), while in the ε-region, concentrated hydrogen solutions with an hcp iron lattice are stable.

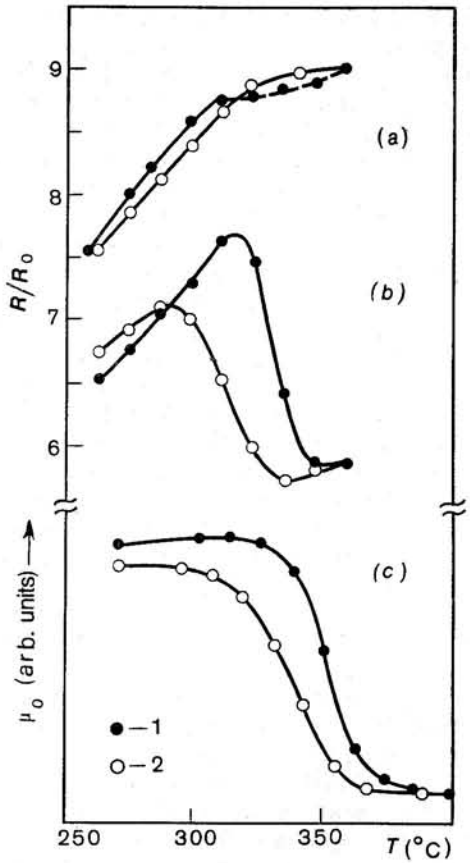

Fig. 4.10. Isobars for the electrical resistance (*a*, *b*; $P_{H_2} = 6.1$ GPa) and initial magnetic permeability (*c*; $P_{H_2} = 5.7$ GPa) in the vicinity of the $\varepsilon \rightleftarrows \gamma$ transformation in the Fe-H system [4.31].
1—upon heating; *2*—upon cooling; *a*—first cycle of heating and cooling; *b*—fifth cycle; *c*—fourth cycle. R_0 is the same as in Fig. 4.3.

The composition and crystal structure of the γ-solutions have not been investigated so far. It is possible, however, to argue in favour of the fact that the γ-phase must be an interstitial hydrogen solution on the basis of an fcc iron lattice. (1) The inset in Fig. 4.8 shows the T-P diagram for iron [4.32], where α, ε, and γ denote the regions of stability of the phases with bcc, hcp, and fcc lattices respectively. The effect of hydrogen on the polymorphic transformations in iron can be estimated from the data for alloys of iron with other transition metals whose addition shifts these transformations to the temperature and pressure regions convenient for measurements. Inves-

tigations of iron-rich Fe-Ni alloys [4.33] and $Fe_{78}Mn_{22}$ alloy have shown [4.34] that temperatures of the $\alpha \rightarrow \gamma$ and $\gamma \rightarrow \alpha$ transitions decrease, while the temperatures of the $\varepsilon \rightarrow \gamma$ and $\gamma \rightarrow \varepsilon$ transitions increase in a hydrogen atmosphere relative to their values at the same pressure in an inert medium. It can be easily seen that if these tendencies are retained for pure iron as well, the T-P_{H_2} diagram of the Fe-H system must have the same topology as the T-P diagram of iron, albeit with a lower pressure at the triple point ($\alpha + \varepsilon + \gamma$). The experiment yields just this type of diagram, see Fig. 4.8. (2) All hydrides of the group VI-VIII transition metals obtained so far are interstitial hydrogen solutions on the basis of just two closest packings of metal atoms, either hcp or fcc (see Table 4.1). (3) The $\varepsilon \rightarrow \gamma$ and $\gamma \rightarrow \varepsilon$ transitions in the Fe-H solutions are accompanied by the resistance anomalies (Fig. 4.10) of the same type as for hcp $\rightleftarrows$ fcc transformations in iron [4.35], Fe-Ru alloys [4.36], Fe-Mn alloys and hydrogen solutions based on them [4.34]. Such transformations in these materials are also characterized by the so-called "training" effect observed in the Fe-H system, consisting in a considerable increase in the amplitude of the resistivity anomalies accompanying the $\varepsilon \rightarrow \gamma$ and $\gamma \rightarrow \varepsilon$ transitions upon transferring the sample several times from the ε- to the γ-state and vice versa (see Fig. 4.10).

The ε-hydride of iron is a ferromagnet with a spontaneous magnetization $\sigma_0 \approx 2.2\ \mu_B$ per Fe atom at atmospheric pressure and $T = 0$ K [4.37], which is close to the σ_0 value for the initial α-Fe. Measurements of magnetic permeability have shown that at $P_{H_2} \leqslant 6.7$ GPa, the ε-solutions Fe-H remain ferromagnetic at all temperatures right up to the temperature of the $\varepsilon \rightarrow \gamma$ transition (typical isobars of the magnetic permeability of the Fe-H solutions in the vicinity of the $\varepsilon \rightleftarrows \gamma$ transformation are shown in Fig. 4.10).

Co-H. Cobalt has two allotropic modifications at atmospheric pressure. At low temperatures, the phase with an hcp lattice is stable, while upon increasing the temperature to $T_\gamma \approx 450°$ C, a transition to the phase with an fcc lattice takes place. In an inert atmosphere, T_γ increases with pressure with a slope $(dT_\gamma/dP)_{in} \approx 33°\ C \cdot GPa^{-1}$ [4.38, 39]. Measurements in a hydrogen atmosphere have shown that at $P_{H_2} \leqslant 2.5$ GPa, the dissolution of hydrogen in cobalt results in a higher $\varepsilon \rightarrow \gamma$ transition temperature as compared to its value in an inert atmosphere at the same pressure [4.39]. At $P_{H_2} \leqslant 6.5$ GPa and $T < T_\gamma$ (P_{H_2}), hydrogen forms with cobalt continuous ε-solutions whose concentration reaches $n \approx 0.5$ at $P_{H_2} = 6.5$ GPa and $T = 225°$ C. An extension of the range of investigation of the Co-H system to $P_{H_2} = 9$ GPa revealed that at $250° \leqslant T \leqslant 350°$ C and $P_{H_2} \approx 7$GPa, this system undergoes the $\varepsilon \rightarrow \gamma$ transorfmation accompanied by an abrupt increase in the solubility of hydrogen in cobalt (Fig. 4.11) and the appearance of an anomaly in the electrical resistance isotherms (Fig. 4.12).

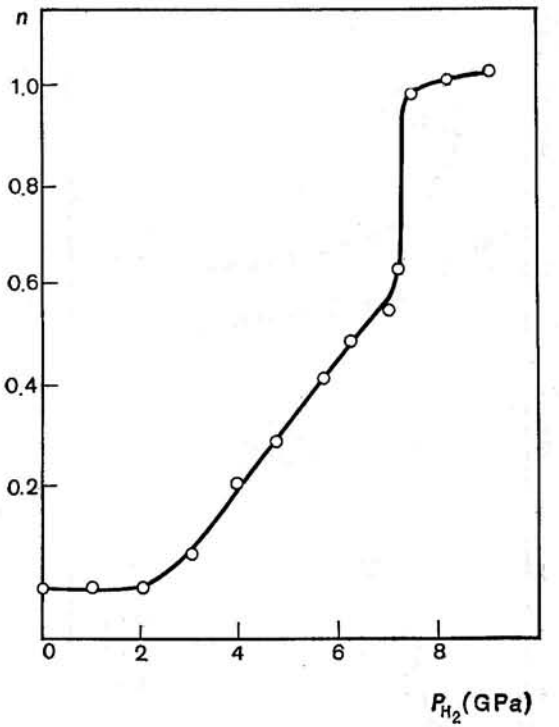

Fig. 4.11. Solubility of hydrogen in cobalt at $T = 350°$C (results of the present paper).

Figure 4.13 depicts the data of X-ray investigations of the Co-H samples saturated with hydrogen at high pressure and $250° \leqslant T \leqslant 350°$ C over a period of 24 hours. Extrapolation of approximately linear a_ε (n) and c_ε (n) dependences from $n \leqslant 0.6$ to $n = 1$ gives the value $\Delta V_\varepsilon \approx 1.82$ Å^3 per Co atom for the increase in the volume of the ε-solutions Co-H upon hydrogenation. It is interesting to note that if the obtained γ-hydride with $n \approx 1$ is treated as a solution of hydrogen in the γ-phase of Co, the increase in the volume upon its formation will have approximately the same value $\Delta V_\gamma \approx 1.8$ Å per Co atom. Since the specific volumes of the ε- and γ-phases of cobalt are also nearly the same, the data obtained on the solubility of hydrogen in these phases permits an analysis of the possible shape of the T-P_{H_2} diagram for the Co-H system.

Indeed, in view of the large specific volume of molecular hydrogen, the formation of the Co-H solid solutions is accompanied by a decrease in the volume of the system. Hence, for given T and P_{H_2}, the thermodynamic equilibrium will shift towards the formation of such

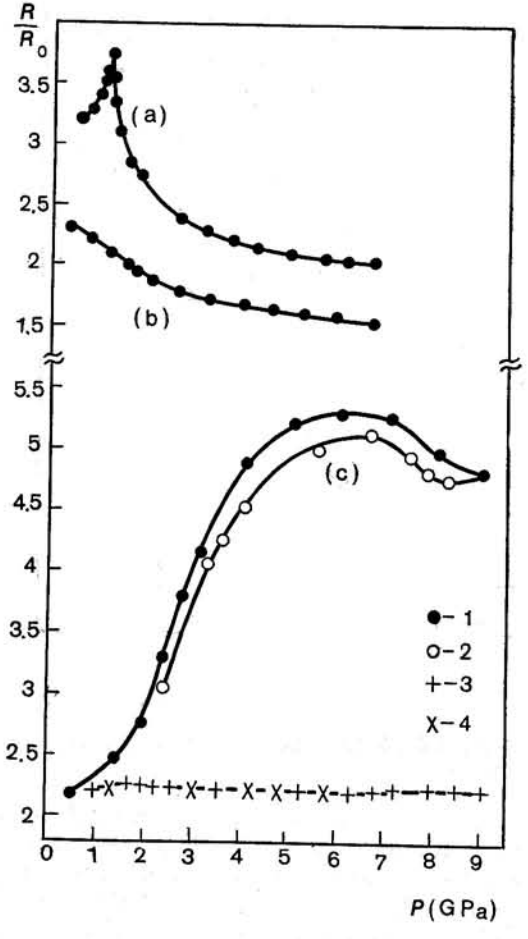

Fig. 4.12. Electrical resistance isotherms for nickel (*a*; $T = 300$°C), palladium (*b*; $T = 200$°C); and cobalt (*c*; $T = 250$°C) (results of the present paper).
1, *2*—with increasing and decreasing pressure in hydrogen atmosphere; *3*, *4*—the same in an inert medium.

solid solutions in which the hydrogen concentration is higher. According to the data given in [4.40], the γ-solutions of hydrogen based on the Ni-Co alloys containing up to 60 at.% Co undergo the isomorphic $\gamma_1 \rightarrow \gamma_2$ transition accompanied by an abrupt increase in the solubility of hydrogen (the T-P_{H_2} diagram for the $Ni_{40}Co_{60}$-H system is presented in Fig. 4.15). An extrapolation to pure cobalt shows that for the γ-solutions Co-H, the line of this transition on the virtual

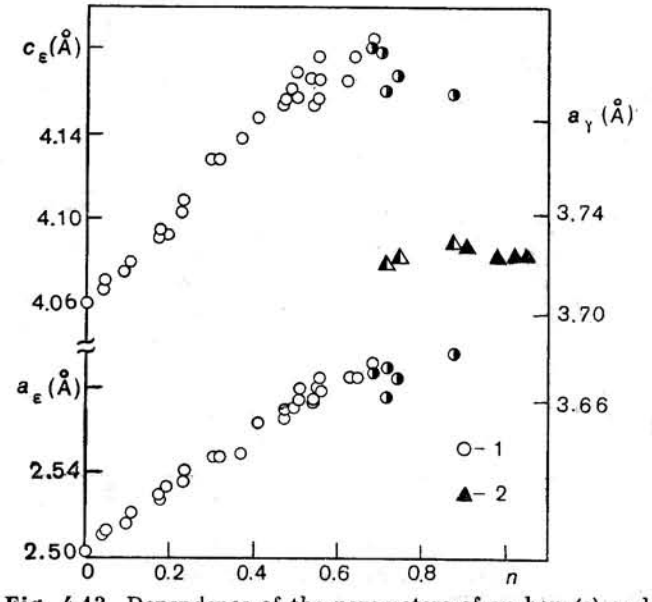

Fig. 4.13. Dependence of the parameters of an hcp (ε) and fcc (γ) metal lattice for Co-H solutions under atmospheric pressure and $T = -190$°C (results of the present paper).
1—ε-solutions; *2*—γ-solutions. The half-filled symbols correspond to the two-phase (ε + γ) samples.

T-P_{H_2} diagram should be close to the vertical $(P_{H_2})_{\gamma_1 \rightarrow \gamma_2} \approx 6$-8 GPa. Thus, while for $P_{H_2} \geqslant 7$ GPa the solubility of hydrogen in γ-Co is higher than in ε-Co (see Fig. 4.11), the situation will most probably be reversed at lower pressures. The following pattern for the $\varepsilon \rightarrow \gamma$ transition temperature in cobalt with increasing hydrogen pressure can therefore be expected: for $P_{H_2} \ll 7$ GPa, the transition temperature should initially increase relative to its value in an inert medium at the same pressure (in other words, the temperature range for the stability of the ε-solutions Co-H should become wider), attain a maximum value, and then rapidly fall at $P_{H_2} \rightarrow (P_{H_2})_{\gamma_1 \rightarrow \gamma_2} \approx 7$ GPa. The available experimental data confirm such a trend in the T_γ (P_{H_2}) dependence.

Ni-H. Nickel hydride was first obtained by electrochemical methods [4.41]. Later, it was also synthesized under equilibrium conditions, i.e. at a high hydrogen pressure [4.42]. At room temperature, nickel hydride is formed through the isomorphic $\gamma_1 \rightarrow \gamma_2$ transition accompanied by an abrupt increase in the solubility of hydrogen in nickel from $n \leqslant 0.01$ to $n \approx 1$. Under normal conditions, nickel hydride is unstable and completely decomposes over a period of a few days.

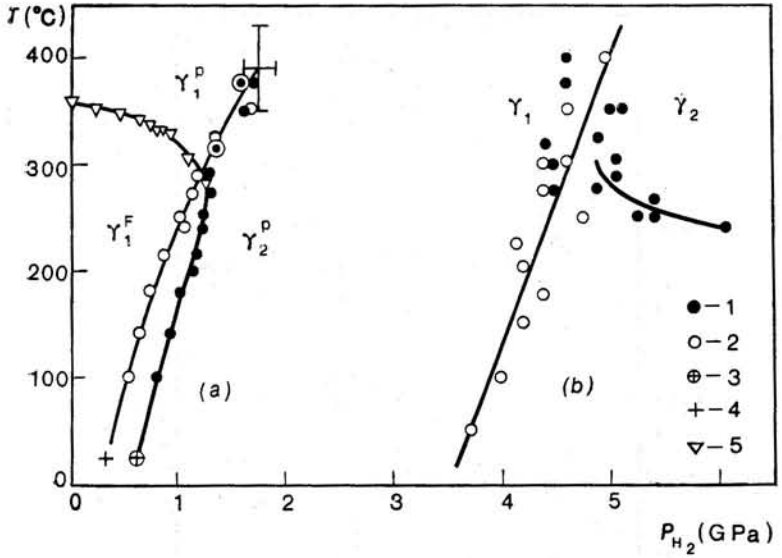

Fig. 4.14. T vs. P_{H_2} phase diagrams for Ni-H [4.43, 13] (*a*) and Rh-H [4.47] (*b*) systems.
1, *2*—pressures corresponding to $\gamma_1 \rightarrow \gamma_2$ and $\gamma_2 \rightarrow \gamma_1$ transitions respectively; *3*, *4*—the same (results of [4.53, 114]); *5*—Curie points; γ^F and γ^P represent the ferromagnetic and paramagnetic phases, respectively.

The T-P_{H_2} phase diagram for the Ni-H system [4.43, 13] is shown in Fig. 4.14. The values of pressures corresponding to the $\gamma_1 \rightarrow \gamma_2$ and $\gamma_2 \rightarrow \gamma_1$ transitions were obtained from the position of anomalies on the electrical resistance isotherms (a typical R vs. P_{H_2} isotherm is presented in Fig. 4.12). It can be seen from Fig. 4.14 that the hysteresis in the $\gamma_1 \rightleftarrows \gamma_2$ transformation declines with a rise in temperature and completely disappears at $T \geqslant 270°$ C. In turn, the maximum solubility of hydrogen in the γ_1-phase increases while its minimum solubility in the γ_2-phase decreases with temperature [4.13], and at $T_{cr} \approx 390°$ C and $(P_{H_2})_{cr} \approx 1.75$ GPa, the line of the $\gamma_1 \rightleftarrows \gamma_2$ phase transformation terminates at a critical point of the liquid-vapour type (the coordinates of the critical point are obtained by extrapolating the data for Ni-Fe-H solutions [4.44]).

Nickel is a ferromagnet with its Curie point at $T_C \approx 354°$ C, and in the region of existence of the γ_1-phase on the T-P_{H_2} diagram for the Ni-H system, an additional curve of Curie points appears [4.43], above which the γ_1-solutions are paramagnetic and below which they are ferromagnetic (the γ_2-solutions are paramagnetic down to liquid-helium temperatures [4.45]). A considerable lowering of Curie points (by $\sim 76°$ C at $P_{H_2} = 1.25$ GPa) for the γ_1-solutions Ni-H with increasing pressure is due to an increase in the equilibrium solubility of hydrogen in nickel, since in an inert medium the Curie point of nickel rises by about 4° C at $P = 1.25$ GPa, see [4.46]. The high sensitivity of Curie points to the hydrogen content of the γ_1-solutions Ni-H is worth noting: at $P_{H_2} = 1.25$ GPa and $T = 270°$ C, the hydrogen concentration in the solution is just $n \approx 0.02$.

Under atmospheric pressure and at $T \leqslant -20°$ C (when the samples are hindered from exchanging hydrogen with the surroundings), the maximum solubility of hydrogen in the γ_1-phase of the Ni-H solutions amounts to $n_{\gamma_1}^{max} \leqslant 0.02$. At $n_{\gamma_1}^{max} < n < n_{\gamma_2}^{min} \approx 0.7$, the samples consist of a mixture of the γ_1- and γ_2-phases with compositions $n_{\gamma_1}^{max}$ and $n_{\gamma_2}^{min}$, while at $n_{\gamma_2}^{min} \leqslant n \leqslant 1.25$, the γ_2-phase is stable [4.45]. At atmospheric pressure and $T = -190°$ C, the parameter a for the fcc metal lattice of the γ_2-solutions Ni-H is approximately equal to 3.72 Å and remains practically unchanged over a wide range of concentrations ($0.7 \leqslant n \leqslant 1.25$). Experimental investigations have revealed that nickel hydride with $n = 1.18$ is not superconducting at temperatures above 1.2 K [4.13].

Ru-H. Ruthenium has an hcp lattice. At $T = 250°$ C, the solubility of hydrogen in ruthenium monotonically increases with pressure and attains the value $n \approx 0.03$ at $P_{H_2} = 9$ GPa. The electrical resistance isotherms for ruthenium in hydrogen and in an inert medium are shown in Fig. 4.7. Under normal conditions, the Ru-H samples are unstable with respect to decomposition into the metal and molecular hydrogen.

Rh-H. Rhodium hydride was first synthesized under high hydrogen pressure [4.19]. The T-P_{H_2} phase diagram for the Rh-H system was constructed in [4.47] from a location of abrupt changes in the electrical resistance isotherms (typical isotherms are shown in Fig. 4.3) and is presented in Fig. 4.14. Our recent measurements have revealed that the $\gamma_1 \rightarrow \gamma_2$ transition is accompanied by an abrupt increase in the solubility of hydrogen in fcc rhodium from $n \approx 0.01$ to $n \approx 1$.

The decomposition of the hydride into the metal and molecular hydrogen begins under atmospheric pressure at $T \geqslant -100$ to $-60°$ C. At $T = -190$ °C, the period of the fcc metal lattice of rhodium hydride with $n = 1.02 \pm 0.03$ is $a = 4.020$ Å. A superconducting transition in rhodium hydride was not observed at temperatures down to 2 K.

Pd-H. Palladium hydride was first synthesized through a direct interaction of the metal with hydrogen and was fairly widely investigated even in the 19th century [4.48]. Like nickel, palladium forms a wide range of interstitial solid solutions with hydrogen on the basis of an fcc lattice of the metal. The T-c diagram of the Pd-H system shows a hump of stratification into the isomorphic γ_1- and γ_2-phases

(depleted and enriched in hydrogen). The parameters of the critical point are given by $T_{cr} = 292°$ C, $(P_{H_2})_{cr} = 1.97$ MPa, and $n_{cr} = 0.25$ [4.11]. Above room temperature and at hydrogen pressures up to 6.7 GPa, other transformations in the Pd-H system do not take place and the solubility of hydrogen in palladium simply increases monotonically with pressure [4.12]. Figure 4.12 demonstrates a typical isotherm for the electrical resistance of the γ_2-solution Pd-H. It is interesting to note that while a hydrogen pressure of just 1 kPa (at room temperature) is sufficient to obtain a Pd-H solution with $n \approx 0.6$, solutions with $n > 1$ cannot be synthesized even at $P_{H_2} = 7$ GPa.

During the last decades, the Pd-H system has attracted the attention of a large number of research workers due to the discovery of the so-called "55 K anomaly" in the temperature dependence of the specific heat of the γ_2-solutions with $n \lesssim 0.8$ [4.49], as well as the discovery of superconductivity in the solutions with $n \gtrsim 0.8$ [4.50]. A detailed description and discussion of the results of investigations in the Pd-H system can be found in the review articles [4.11, 51].

Os-H. This system is completely analogous to the Ru-H system, the only difference being that at $T = 250°$ C and $P_{H_2} = 9$ GPa, the solubility of hydrogen in osmium is about ten times lower than in ruthenium and constitutes $n \approx 0.003$.

Ir-H and Pt-H. Iridium and platinum are metals with an fcc lattice. The concentration of hydrogen in samples obtained by keeping 0.1 mm thick foils of these metals under a hydrogen pressure of 9 GPa at $T = 250$ °C attained the value $n \approx 0.005$. Under atmospheric pressure and at room temperature, all the hydrogen is liberated from the samples over a few minutes. It should, however, be noted that the electrical resistivity of iridium and platinum in hydrogen at 250° C behaved practically in the same manner as in an inert atmosphere (see Fig. 4.7). In this respect, it remains unclear whether hydrogen was actually dissoluted in the bulk of the metal or whether there was, say, just an adsorption of hydrogen over macroscopic defects in the course of the experiment.

Ni-Me-H systems. The main body of data on the magnetic properties of hydrides of transition metals, which are described and analysed in Sec. 4.4, was obtained from an investigation of the solutions of hydrogen in the alloys of nickel with Cu, Co, Fe, Mn, and Cr. Hence, it is expedient to briefly describe the changes introduced in the structure and phase composition of the solutions as a result of replacing nickel by these metals.

Nickel forms a wide range of disordered substitutional solid solutions with these metals on the basis of an fcc lattice [4.52]. During the formation of the Ni-Me-H solutions, hydrogen occupies the interstices in this lattice. Substitution of nickel by other metals leads to a smooth deformation of the T-P_{H_2}-c diagram of the Ni-H system, the

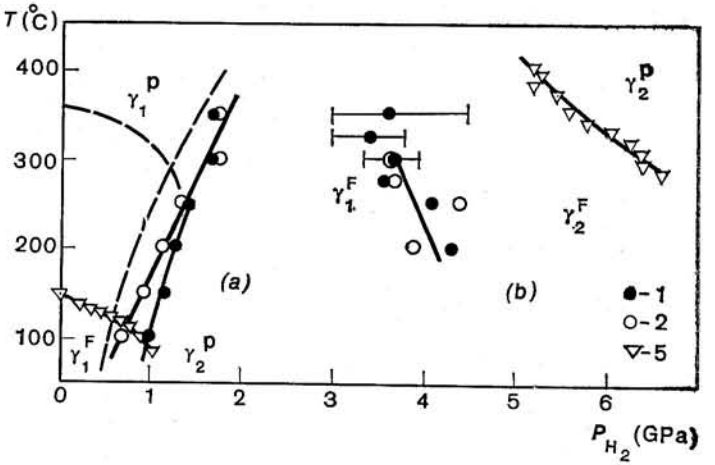

Fig. 4.15. T vs. P_{H_2} phase diagrams for the $Ni_{95}Cr_5$-H system (results of the present paper) (*a*), and $Ni_{40}Co_{60}$-H system [4.40] (*b*). The notation is the same as in Fig. 4.14. The dashed lines show the curve for $\gamma_2 \rightarrow \gamma_1$ transitions and the Curie temperature line for the system Ni-H [4.43, 13].

critical temperature of stratification into the γ_1- and γ_2-phases decreasing in all cases. By way of an illustration of the observed effects, Fig. 4.15 shows the variation of the T-P_{H_2} diagram of the Ni-H system when nickel is replaced by cobalt and chromium. In particular, it can be seen from Fig. 4.15 that doping by these metals shifts the line of the $\gamma_1 \rightleftarrows \gamma_2$ phase transformation towards the region of higher pressures. The addition of iron has a similar effect on the pressure of the $\gamma_1 \rightleftarrows \gamma_2$ transformation [4.44, 53], while a substitution of nickel by copper [4.54, 55] or manganese [4.56, 57] practically does not change the position of the line of the $\gamma_1 \rightleftarrows \gamma_2$ transformation on the T-P_{H_2} diagram. If nickel contains more than $\sim$ 40 at. % Cu, $\sim$ 15 at. % Fe, or $\sim$ 20 at. % Mn, the critical temperature of phase separation in the corresponding Ni-Me-H systems falls below room temperature and at $T \gtrsim 25°$ C, the solubility of hydrogen in alloys with a larger concentration of the doping element becomes a continuous function of pressure. Investigations of the Ni-Me-H samples, which were preliminarily saturated with hydrogen at high pressures and which were metastable at atmospheric pressure, showed that at $P \approx 0.1$ MPa, the critical temperature falls below the room temperature at lower concentrations of the doping metal (for example, a separation into the γ_1- and γ_2-phases in the case of Ni-Fe-H solutions [4.58] was not observed even in $Ni_{90}Fe_{10}$-H samples).

The dependences of increase in the volume of an elementary cell on hydrogen concentration are similar for the γ-alloys Ni-Me. For

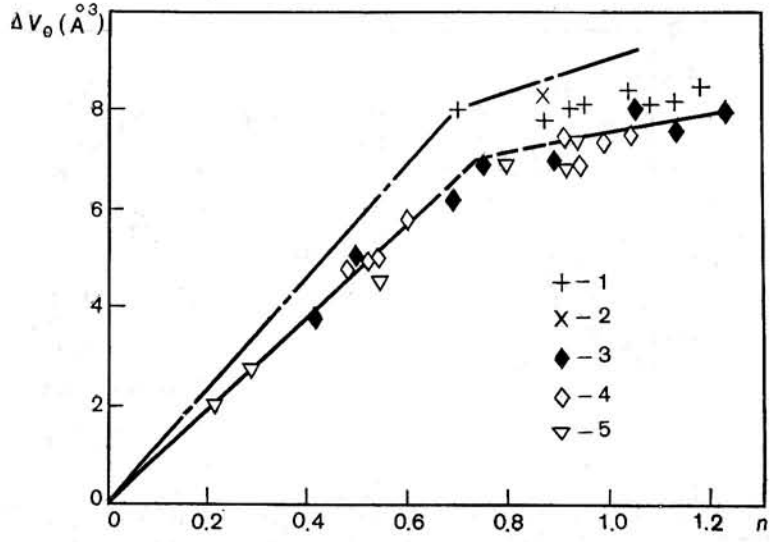

Fig. 4.16. ΔV_0 vs. n dependence for the increase in the volume of unit cell for fcc metals and alloys.
1—Ni, $T = 293$ K [4.13]; *2*—Ni, $T = 293$ K [4.115]; *3* and *4*—Ni-Fe alloys with 20 and 67.6 at. % Fe respectively, $T = 83$ K [4.58]; *5*—$Fe_{65}Ni_6Mn_{29}$, $T = 83$ K [4.83]; the dot-and-dash line shows the ΔV_0 (n) dependence for palladium-based alloys at room temperature [4.59].

most of the alloys, these dependences have a common feature: at $n \gtrsim 0.7$-0.8, a decrease in their slope $\beta = (\partial/\partial n)\,\Delta V_0$ (n) is observed. For example, the slope for the $Ni_{80}Fe_{20}$ and $Ni_{32.5}Fe_{67.5}$ alloys changes from $\beta \approx 9.5$ Å^3 for $n < 0.8$ to $\beta \approx 2.5$ Å^3 for $n > 0.8$, see Fig. 4.16 (for the sake of clarity, the ΔV_0 vs. n dependence for $n < 0.8$ and $n > 0.8$ is approximated by straight line segments). A similar trend was earlier observed for the ΔV_0 vs. n dependence for palladium-based alloys [4.59]. The nature of this effect is not yet understood. Some possibilities for explaining it are opened up by the investigations of hydrogen solutions in nickel and nickel-based alloys, for which the concentrations $n > 1$ has been obtained. Indeed, for $n \approx 0.6$ and at room temperature, hydrogen in nickel occupies octahedral interstices [4.60] whose number in an fcc lattice is equal to the number of lattice points. When all these interstices are filled in, the γ-hydride will have a concentration $n = 1$. Consequently, γ-solutions with $n > 1$ must be different in structure as compared to solutions with $n \approx 0.6$. The only anomaly in the ΔV_0 vs. n dependences for the Ni-H and Ni-Me-H γ-solutions at hydrogen concentrations up to 1.23 (for the $Ni_{80}Fe_{20}$-H solution) is observed at $n \approx 0.8$, and it is logical to assume that this anomaly is due to the on-

set of a structural rearrangement. As to the rearrangement, it may involve, for example, the occupation of a part of the tetrahedral interstices for $n > 0.8$, whose number in an fcc lattice is equal to two per lattice point (although in this case, due to the smaller dimensions of the tetrahedral pores, the partial volume of hydrogen, characterized by the value of β, is more likely to increase than decrease). It also cannot be excluded that even for $n > 0.8$, hydrogen continues to occupy only octahedral interstices whose number per lattice point increases due to an increase in the number of vacancies in the fcc lattice of the metal for $n > 0.8$.

In conclusion of this section, it is worth noting that upon a decrease in temperature even down to $T \leqslant 4.2$ K, none of the investigated samples of nonstoichiometric solid solutions Ni-Me-H revealed an ordering or a separation into phases of stoichiometric (with respect to hydrogen) composition. Generally speaking, such phenomena could be expected from the requirement of minimum configurational entropy. This is probably due to the fact that the corresponding critical temperatures are very low and thermodynamically equilibrium states are not attained for kinetic reasons.

4.4. MAGNETIC PROPERTIES OF METAL-HYDROGEN SOLUTIONS

The 3*d*-metals of VI-VIII groups and alloys based on these metals are characterized by the existence of a magnetic order. Experiments have shown that in the case of transition metals, hydrogenation does not lead to a unique variation of their magnetic properties, for example, to a decrease in the temperature of transition to the magnetically ordered state, which is a dominating trend in the case of hydrogenation of rare-earth metals [4.61]. On the contrary, the effects have turned out to be very diverse. In particular, the following phenomena are observed upon hydrogenation of pure metals.

Chromium, which has a bcc lattice, is an antiferromagnet with the Néel temperature $T_N = 312$ K; the ε-hydride $CrH_{0.97}$ is paramagnetic down to helium temperatures [4.62, 63]. The low-temperature modification of manganese (α-Mn) is an antiferromagnet with $T_N = 100$ K; in the concentration range of $0.65 \leqslant n \leqslant 0.94$, the ε-solutions Mn-H possess a spontaneous magnetization which increases monotonically with concentration of hydrogen in the solution, but even at $n = 0.94$ remains very small ($\leqslant 0.02$-$0.05\mu_B$ per Mn atom at $T = 82$ K; μ_B is the Bohr magneton), while the Curie point attains quite high values $T_C > 280$ K [4.27]. Iron with a bcc structure is a ferromagnet with $T_C = 1043$ K, which has at $T = 0$ K a spontaneous magnetization $\sigma_0 = 2.22$ μ_B per atom; the ε-hydride $FeH_{0.8}$ is also

a ferromagnet with nearly the same value of $\sigma_0 = 2.2\mu_B$ per Fe atom [4.37] and with $T_C > 670$ K [4.31, 37]. Dissolution of hydrogen in the hcp modification of cobalt (ferromagnet with $\sigma_0 = 1.72$ μ_B per atom) leads to a slight decrease in the spontaneous magnetization (see [4.64], and also Fig. 4.26). Fcc nickel is a ferromagnet with $T_C = 627$ K and $\sigma_0 = 0.616$ μ_B per atom. Introduction of hydrogen causes a decrease in the value of T_C (see Fig. 4.14) and also lowers the magnetization σ_0; in the concentration range $0.7 \leqslant n \leqslant 1.18$, the γ_2-solutions Ni-H are paramagnetic at $T \geqslant 4.2$ K [4.45].

A simple listing of the above facts already indicates that it is, in any case, not easy to construct a consistent picture of the effect of hydrogen on the magnetic properties of transition metals, limiting the study to the properties of Me-H solutions based on the elements only. In this connection, it was very fruitful to investigate the hydrogen solutions in fcc alloys of 3*d*-metals, and, primarily, in the nickel-based alloys. Nickel-based alloys have for a long time been the subject of intensive experimental investigations, and the large body of experimental data accumulated over the years provides an exact picture of the effect of the doping substitution elements on the magnetic properties of materials (see [4.65, 66]). The alloys form a wide range of continuous γ-solutions with hydrogen, which permits a systematic investigation of the effect of the addition of hydrogen on these properties. Finally, the magnetic properties of fcc alloys based on nickel are correctly described by the band theory of magnetism, thus creating a proper base for the interpretation of the effects arising as a result of hydrogenation.

4.4.1. Magnetic Properties of Ni-Me Alloys

In the band theory of magnetism, the electrons, which partially fill the conduction band, are the carriers of the magnetic moment. The exchange interaction leads to the dependence of the energy of the electrons on the orientation of their magnetic moment which, in the first approximation, can be represented as the relative shift of the electron subbands for opposite directions of spins by the energy $\Delta = I\sigma$, where I is the effective exchange interaction parameter. Usually, it is assumed that the Fermi level in transition metals intersects the overlapping narrow *d*-band (with a high density of electron states) and the wide *s*-band (with a low density of states), the magnetic properties of the material being mainly determined by the structure of the *d*-band and the degree to which it is filled. It should be noted that in spite of the evident roughness of these approximations, such an approach permits a quantitative description of the temperature, field, pressure, and concentration dependences of the macroscopic magnetic characteristics in the case of fcc alloys based on 3*d*-metals (see, for example, [4.65-68]).

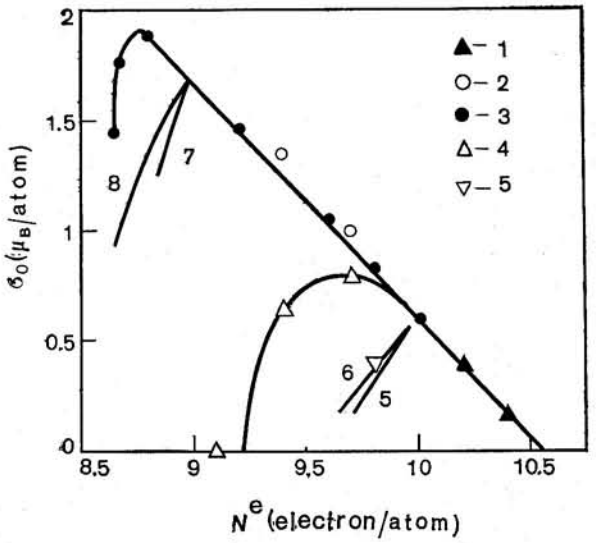

Fig. 4.17. Spontaneous magnetization σ_0 at $T = 0$ K as a function of the average number N^e of $(3d + 4s)$ electrons per atom in binary fcc alloys (see [4.65, 66]).
1—Ni-Cu; *2*—Ni-Co; *3*—Ni-Fe; *4*—Ni-Mn; *5*—Ni-Cr; *6*—Ni-V; *7*—Co-Cr; *8*—Co-Mn.

The dependence of spontaneous magnetization σ_0 on concentration at 0 K for fcc alloys of *3d*-metals is customarily represented in the form of the Pauling-Slater curve (Fig. 4.17) as a function of the average number N^e of $3d + 4s$ electrons (present in an isolated atom) per atom of the alloy. Figure 4.17 shows the experimental values of σ_0 for Ni-Me alloys serving as a basis for obtaining the solid hydrogen solutions considered in this paper.

The following characteristic property of the Pauling-Slater curve is worth noting: the values of σ_0 for the alloys of nickel with cobalt, copper and iron (for atomic fraction of iron $x_{Fe} \leqslant 0.6$) fall on a single straight line with a slope $\partial\sigma_0/\partial N^e \approx -1.05$ μ_B per electron. Nickel is well described by the band theory of ferromagnetism, and near 0 K it can be considered as a strong itinerant ferromagnet for which one half of the *d*-band ($d\uparrow$ with spins pointing up) is filled completely, while the other half ($d\downarrow$ with spins pointing down) is only partially filled [4.68]. This is shown schematically in Fig. 4.18*a*. The magnitude of σ_0 is related to the number of electrons with uncompensated spin, i.e., in this case, simply to the number of holes $p\downarrow$ in the $d\downarrow$-subband, through the relation $\sigma_0 = (1/2)g\mu_B \cdot p\downarrow \approx \mu_B p\downarrow$, since for nickel (and for alloys based on nickel) the spectroscopic factor $g \approx 2.2 \sim 2$, see [4.66] (which indicates the smallness of the or-

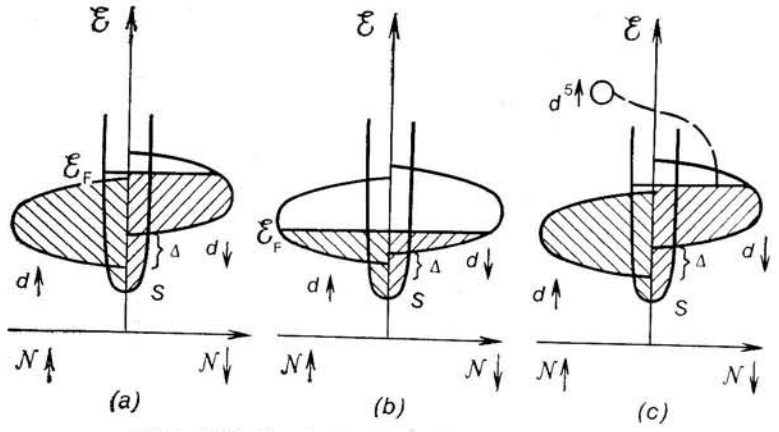

Fig. 4.18. Band structure diagrams for itinerant ferromagnets at $T = 0$ K.
a—strong ferromagnet; *b*—weak ferromagnet; *c*—diagram illustrating the flow of electrons from the virtual impurity bound state $d^5\uparrow$ to the $d\downarrow$-subband of a strong ferromagnet. $\mathscr{E}$ is the energy of states; $\mathscr{N}\uparrow$ and $\mathscr{N}\downarrow$ represent the density of states with upward and downward spins; $\mathscr{E}_F$ is the Fermi energy; $\Delta = I\sigma_0$.

bital contribution, i.e. nearly pure spin origin of magnetization in these materials). The linear dependence of σ_0 on N^e with a slope $\partial\sigma_0/\partial N^e \approx -1\mu_B$ per electron for the alloys of nickel with Cu, Co, and Fe are well explained if it is assumed [4.65] that alloying nickel with these elements (1) does not lead to deformation of the curves for the density of electron states $\mathscr{N}\uparrow(\mathscr{E})$ and $\mathscr{N}\downarrow(\mathscr{E})$, only shifting them in energy, relative to one another, as a single entity (this approximation is called the rigid band approximation for ferromagnets; the physical significance of this approximation and the limits of its applicability are discussed in [4.66]). (2) The alloys remain strong ferromagnets (with completely filled $d\uparrow$-subband). Indeed, in this case, the changes in σ_0 upon doping will stem primarily from the change in the number of holes in the $d\downarrow$-subband and, hence,

$$\sigma_0(x_{Me}) \approx \sigma_0^{Ni} + \Delta Z \mu_B x_{Me}, \qquad (4.1)$$

where $\Delta Z = Z_{Ni} - Z_{Me}$ is the difference in the nuclear charges of nickel and the impurity. This is what as actually observed in experiments.

As can be seen from Fig. 4.17, the behaviour of the dependence of σ_0 on N^e for many alloys deviates from that predicted by the rigid band model for strong itinerant ferromagnets. For Ni-Fe alloys with $x_{Fe} \geqslant 0.63$, this deviation is apparently related to the appearance of a significant number of holes in the $d\uparrow$- as well as in the $d\downarrow$-subbands [4.70]. The corresponding band scheme is shown in Fig. 4.18*b*.

The fact that the spontaneous magnetization may decrease rather than increase with increasing number of holes in the *d*-band in itinerant ferromagnets with holes in both *d*-subbands at $T = 0$ K (such ferromagnets are called weak) can be illustrated in the following manner. Let, as in Fig. 4.18*b*, $\mathscr{N}\uparrow(\mathscr{E}_F) > \mathscr{N}\downarrow(\mathscr{E}_F)$, where $\mathscr{E}_F$ is the Fermi level. Then, with a decrease in the occupancy of the *d*-band by electrons, the number of holes in the $d\uparrow$-subband will rise more rapidly than in the $d\downarrow$-subband, and $\sigma_0 = (1/2)\, g\mu_B\,(p\downarrow - p\uparrow) \approx \mu_B\,(p\downarrow - p\uparrow)$ will decrease.

The "anomalous" dependences of σ_0 on N^e, like those observed for Ni-Cr and Ni-V alloys, when the strong deviation from the straight line with a slope $\partial\sigma_0/\partial N^e \approx -1\mu_B$ per electron appears already at low concentrations of the doping element, were explained by Friedel [4.69] by using the concept of "virtual bound states". According to Friedel, when an atom of a transition impurity appears in a metal, the *d*-level of this atom, which is higher in energy than the bottom of the conduction band, becomes delocalized. However, in the space of coordinates and energy there remains a "virtual *d*-level", viz. the region where (1) the amplitude of the spherical component of the wave function with $l = 2$ is anomalously large, and (2) this amplitude corresponds to the excess charge density, which, being summed over the entire region, is approximately equal to the charge of the initial bound *d*-state (which is $2l + 1 =$ five-fold degenerate). This virtual level may split into sublevels with opposite spins due to the intra-atomic exchange interaction, if the metal-solvent has a sufficiently narrow conduction band (and more so, if it is a ferromagnet).

In the case of nickel, as long as the virtual $d^5\uparrow$-sublevel lies below the Fermi level, alloying will lead to changes as in the rigid band model for strong itinerant ferromagnets (see (4.1)). This is due to the fact that screening of the excess impurity charge is mainly ensured by a part of the *d*-band with a high density of states at the Fermi level, i.e. by the d$\downarrow$-subband, the characteristic screening radius being less than or of the order of the interatomic distance [4.69]. Therefore, the magnetic moments of the nickel matrix and of the impurity must be independent of the impurity concentration:

$$\begin{cases} \mu_{matr} = \text{const}, \\ \mu_{imp} = \mu_{matr} + \Delta Z \mu_B. \end{cases}$$

This leads to the formula (4.1) for the average magnetic moment $\bar{\mu} = \sigma_0$ of the alloy.

The larger the difference ΔZ (i.e. the farther the impurity element is to the left of nickel in the Periodic Table), the higher the perturbing potential (repulsive in nature) introduced by the impurity. It may be expected that for a certain value of ΔZ, this potential will be large enough to take the virtual $d^5\uparrow$-state out of the filled half of

the d-band and to shift it in energy above the Fermi level. This situation is schematically shown in Fig. 4.18*c*. The electrons from such a state pour out into the conduction band and mainly fall into the $d\downarrow$-subband with opposite spin due to its high density of states at the Fermi level (dotted line in Fig. 4.18*c*). The state with $l = 2$ is fivefold degenerate. Consequently, when the virtual $d^5\uparrow$-level crosses the Fermi level, five electrons from the states with upward spin go over into the states with downward spin, thus changing the spontaneous magnetization by $\sim 10\ \mu_B$. This leads to the following formula for the average magnetic moment of the alloy:

$$\sigma_0\,(x_{Me}) \approx \sigma_0^{Ni} + (\Delta Z - 10)\,\mu_B x_{Me}, \qquad (4.2)$$

which is in good agreement with the slopes of the σ_0 vs. N^e dependences for alloys of nickel with chromium, vanadium, and titanium.

Thus, if the impurities are listed in order of decreasing atomic numbers, the following picture is observed when Ni is alloyed with other $3d$-metals. Copper, cobalt, iron, and (partially) manganese do not change the band structure of nickel very much, and over a wide range of the alloy compositions, the σ_0 vs. x_{Me} dependences are determined mainly by changes in the electron concentration N^e. With alloying by elements with $Z < Z_{Cr}$, both changes in N^e and in the band structure play an important role.

4.4.2. Ni-Me-H Solutions

Friedel's analysis of the proton screening conditions in transition metals [4.71] showed that the state of hydrogen in metals at the beginning of the d-series must be closer to H^-, and in metals at the end of these series, to H^+. In recent years, a series of quantum-mechanical calculations of the band structure of hydrides of $3d$- and $4d$-metals, among which the seminal work by Switendick deserves special mention [4.72], have been performed. The results of all the calculations, which were carried out by using different methods (APW method [4.72-75], model Hamiltonian method [4.76]), with a different choice of crystal potentials and self-consistent calculations [4.73, 74], are in good agreement with each other and give for γ- and ε-solutions with $n \leqslant 1$ the following pattern for the effect of hydrogen on the band structure of the metals at the end of the $3d$- and $4d$-series of the Periodic Table. A new hydrogen band below the Fermi level is not formed in such hydrides, i.e the hydrogen states are actually close to H^+ and the hydrogen atoms are electrons donors in the conduction band of the host metal. At the same time, the dissolved hydrogen strongly deforms the band structure of the metal, both the H-Pd and H-H interaction playing an important role. This deformation, however, has a selective character. The d-type states, especially in the upper part of the d-band (which is responsible for the magnetic properties of a material), change only slightly, while the energy of the s-states decreases significantly. The latter leads to an increase in the number of states below the Fermi energy of the host metal with increasing number of protons in its interstices. Thus, only a part of the electrons ($\eta \approx 0.4$-0.1 electron per proton for Pd and Ni [4.72]), supplied by hydrogen atoms to the conduction band, occupies states above the Fermi level, while another part goes into these additional levels below it. Qualitatively, this effect can be illustrated with the help of the diagrams shown in Fig. 4.18, assuming that with increasing hydrogen concentration in the metal, the curve for the density of the s-states is shifted down in energy with respect to the curves for the density of the $d\uparrow$- and $d\downarrow$-states. It should be noted that in view of the high density of the d-states at the Fermi level, nearly all the electrons with energy $\mathscr{E} > \mathscr{E}_F$ of the host metal must occupy just these states, i.e. each hydrogen atom is a donor of η electrons into the d-band of the metal.

Calculations of the band structure of hydrides of transition metals have explained (in many cases quantitatively) the results of the experimental investigation of the electron heat capacity, magnetic susceptibility, photoemission spectra, and other physical properties, including superconductivity, for a number of Me-H systems (see [4.72-74, 76, 11]). For the Ni-Me-H solutions, these calculations have served as a theoretical basis for justifying the use of the "rigid d-band model" to describe their magnetic properties [4.56]. According to this model, the change in these properties upon hydrogenation is mainly caused by the increase in the degree of filling of the d-band of the host metal, hydrogen being considered as the donor of a fractional number of electrons $\eta \leqslant 1$ electron per atom to the d-band. It should, however, be emphasized that such a model is not a direct consequence of band calculations, since the magnetic properties are also affected by a variation in the exchange interaction which is not yet possible to estimate correctly; the strong volume effects accompanying dissolution of hydrogen in Ni-Me alloys must also be kept in mind.

The diversity of the magnetic properties of Ni-Me alloys make them convenient model objects for clarifying various aspects of the influence of hydrogen. We shall now describe the most significant results of experimental investigations of the magnetic properties of a number of Ni-Me-H systems and show that the behaviour of these properties can be unambiguously explained within the framework of the rigid d-band model.

4.4.2.1. Ni-Fe-H system. Figure 4.19 shows the σ_0 vs. n dependences for γ-solutions of hydrogen in nickel [4.45] and Ni-Fe alloys [4.58]. The γ_2-phase of Ni-H solutions is paramagnetic at $T \geqslant 4.2$ K, the minimum solubility of hydrogen in this phase at $T < 250$ K being $n_{\gamma_2}^{min} = 0.7$ [4.45]. Samples with $n < 0.7$ consist of a mixture of γ_1- and γ_2-phases, while their magnetization is proportional to the

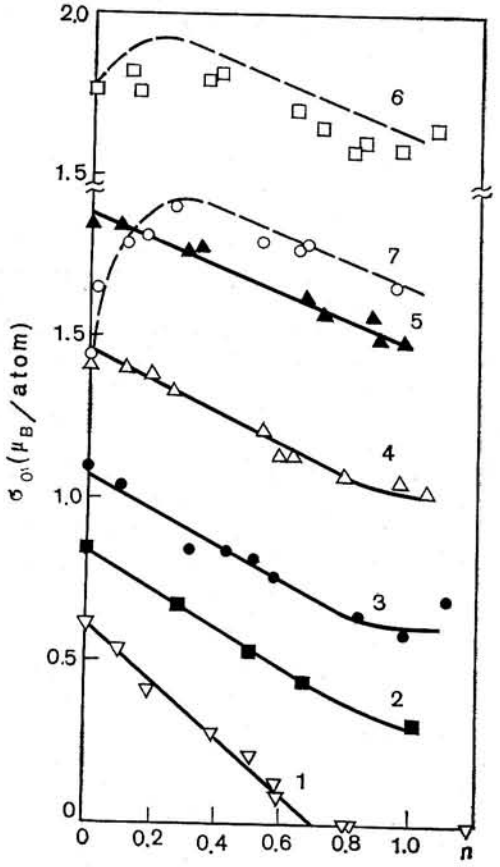

Fig. 4.19. Dependence of the spontaneous magnetization σ_0 at $T = 0$ K and under atmospheric pressure on the hydrogen concentration n in Ni-Fe alloys with different iron contents [4.58]. At. % Fe: *1*—0; *2*—10; *3*—20; *4*—40; *5*—60; *6*—66.1; *7*—67.5. The dashed lines show the σ_0 (n) dependences for alloys with 66.1 and 67.5 at. % Fe, calculated by using the relation (4.4.3). σ_0 is given in μ_B/atom of the Ni-Fe alloy.

content of the γ_1-phase with σ_0 ($n_{\gamma_1}^{max}$) $\approx \sigma_0^{Ni}$. A separation into γ_1- and γ_2-phases was not observed in hydrogen solutions in Ni-Fe alloys with $x_{Fe} \geqslant 0.1$.

The first thing that draws attention in the σ_0 vs. n dependences for the alloys with $0.1 \leqslant x_{Fe} \leqslant 0.6$ is the presence of a linear section for $n \leqslant 0.8$ and deviation from linearity for $n > 0.8$. It should be recalled that the composition $n \approx 0.7$-0.8 is singular for all investigated γ-solutions of hydrogen in nickel- (and palladium-) based alloys:

the nature of the ΔV_0 vs. n dependences changes for $n > 0.8$ (see Fig. 4.16). The reasons behind the appearance of this anomaly are not clear, so it is expedient to confine the discussion to the magnetic properties of Ni-Fe-H solutions with $n \leqslant 0.8$. The values of the slopes $\partial\sigma_0/\partial n$ obtained with a linear approximation to the experimental σ_0 vs. n dependences at $n \leqslant 0.8$ for alloys containing $\leqslant 60$ at. % Fe, decrease monotonically and nearly linearly in absolute magnitude with increasing iron content in Ni-Fe alloys (and, correspondently, with decreasing electron concentration N^e of these alloys) from $\sim 0.6\mu_B$ per H atom for $x_{Fe} = 0.1$ to $\sim 0.4\mu_B$ per H atom for $x_{Fe} = 0.6$.

Ni-Fe alloys with $x_{Fe} \leqslant 0.6$ are strong itinerant ferromagnets. It should be noted that as long as the ferromagnet remains strong (i.e., at $T = 0$ K, holes are present only in its $d\downarrow$-subband), the value $\sigma_0 \propto p\downarrow = p$, viz. the total number of holes in the d-band. So, σ_0 is independent of the change in the exchange interaction and of the deformation of the bands if it does not cause a change in p. In the rigid band approximation ("proton" model), the hydrogenation of such ferromagnets should, therefore, lead to a decrease in their magnetization with a slope $\partial\sigma_0^r/\partial n \approx -1\mu_B$ per H atom. If, as a result of hydrogenation, holes appear both in the $d\downarrow$- and $d\uparrow$-subbands, this will cause a decrease in σ_0 with $|\partial\sigma_0/\partial n| > |\partial\sigma_0^r/\partial n|$, since the lowering of σ_0 due to filling of the $d\downarrow$-subband by the hydrogen electrons will be supplemented by the effect of the transfer of the electrons from $d\uparrow$-subband to $d\downarrow$-subband. For hydrogen solutions in Ni-Fe alloys with $x_{Fe} \leqslant 0.6$, the slopes $|\partial\sigma_0/\partial n| \approx 0.5\ \mu_B$ per H atom are less than $|\partial\sigma_0^r/\partial n|$. It is reasonable to ascribe this to the changes in the band structure of the Ni-Fe alloys occurring upon hydrogenation and accompanied by an increase in the number p of holes in the d-band. In the framework of the rigid d-band model, the experimental values of $\partial\sigma_0/\partial n$ may be explained by considering hydrogen as a donor of a fractional number of electrons $\eta \approx 0.5$ electron per H atom to the d-band of Ni-Fe alloys.

Let us go back to Fig. 4.19. A comparison with Fig. 4.17 shows that for all Ni-Fe alloys with $x_{Fe} \leqslant 0.675$, the concentration dependences of σ_0 with the introduction of hydrogen into the alloys and with the substitution of iron by nickel are similar: for a certain concentration, σ_0 attains its maximum value $\sigma_0^{max} \approx 1.86$-$1.9\mu_B$ per atom, and then begins to decrease. The similarity between σ_0 vs. n dependences for the alloys with 66.1 and 67.5 at. % Fe and the σ_0 vs. x_{Ni} dependence in the Ni-Fe system is even more complete, as can be shown in the following way. For alloys with $x_{Fe} \leqslant 0.6$, the magnetization decreases linearly both when Fe is replaced by Ni and when the hydrogen concentration is increased. Following [4.58], let us introduce for each specific Ni-Fe alloy with $x_{Fe} \leqslant 0.6$, the coefficient ξ, relating the changes in the composition of the binary Ni-Fe alloys

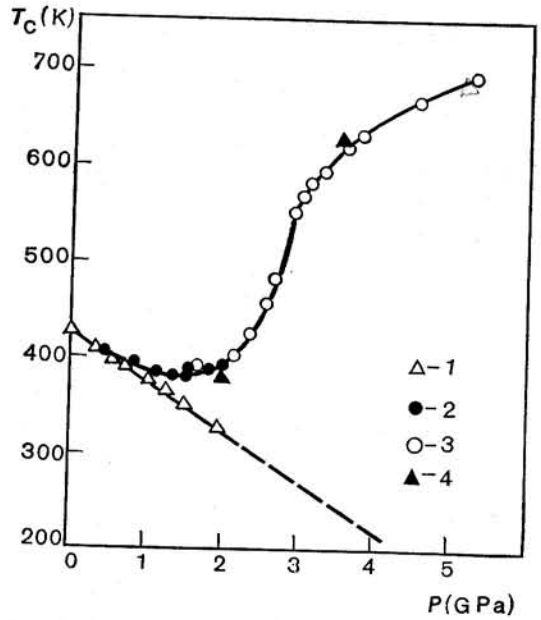

Fig. 4.20. Pressure dependence of the Curie temperatures of $Ni_{67.5}Fe_{32.5}$ alloy in an inert medium (*1*) (results of [4.87]) and in hydrogen (*2*) (results of [4.87]); *3*—results of [4.58]; *4*—values of T_C (n) calculated by using the relations (4.4.3) and (4.4.4).

and changes in n, leading to the same changes in σ_0:

$$\Delta x_{Fe} = \frac{(\partial\sigma_0/\partial n)}{(\partial\sigma_0/\partial x_{Fe})} n = -\xi n. \qquad (4.3)$$

Extrapolation of the approximately linear ξ vs. x_{Fe} dependence to alloys with $x_{Fe} = 0.661$ and 0.675 gives $\xi \approx 0.185$. The σ_0 vs. n dependences for these alloys constructed with such a value of the scaling factor ξ are shown by the dotted lines in Fig. 4.19. It is seen that they are in agreement with the experimental data.

A similar correspondence occurs between the Curie points of the Ni-Fe alloys and hydrogen solutions based on them. The experimental dependences of the Curie points for the alloy with 67.5 at.% Fe on pressure in an inert medium and in hydrogen are shown in Fig. 4.20. It can be seen that in an inert medium, T_C of the alloy decreases linearly with a slope $(dT_C/dP)_{in} \approx -50$ K·GPa^{-1} with pressure up to 2 GPa. In a number of papers (for example, in [4.77]), it is shown that for Ni-Fe Invars the T_C vs. P dependence in an inert medium is nearly linear (dotted line in Fig. 4.20) at higher pressures as well. When measurements are carried out in a hydrogen atmosphere,

the hydrogen concentration in the alloy increases with pressure (right up to $n \approx 1$ at $P_{H_2} = 5.1$ GPa and $T = T_C$ of the $Ni_{32.5}Fe_{67.5}$-H solution at this pressure). This results in a significant deviation in the T_C vs. P_{H_2} dependence from that in an inert medium toward higher temperatures.

Assuming that the correspondence established by formula (4.3) between σ_0 of alloys with and without hydrogen is also valid for T_C and $(dT_C/dP)_{in}$, we get the following relation for Ni-Fe-H solutions:

$$T_C(P_{H_2}) = T_C(x_{Fe} - \xi n) + \left(\frac{dT_C(x_{Fe}-\xi\cdot n)}{dP}\right)_{in} P_{H_2}. \qquad (4.4)$$

The values of T_C (P_{H_2}) for the $Ni_{32.5}Fe_{67.5}$-H solutions, calculated in [4.58] by using formula (4.4), are shown in Fig. 4.20 by solid triangles and are in good agreement with the experimental dependence. It was also shown in [4.58] that the relations (4.3) and (4.4) satisfactorily describe the behaviour of the T_C vs. P_{H_2} dependence for the non-Invar $Ni_{90}Fe_{10}$ alloy as well.

Thus, over the entire investigated concentration range $0.1 \leqslant x_{Fe} \leqslant 0.675$ for the Ni-Fe alloys, the σ_0 (n) and σ_0 (Δx_{Fe}) dependences, as well as the T_C (n) and T_C (Δx_{Fe}) dependences are similar and, in addition, have the same similarity factor ξ. Formally, this can be represented as a similarity in the dependences of σ_0 and T_C on electron concentration upon hydrogenation and upon replacement of Fe by Ni, respectively. The coefficients of such similarity, $\zeta = (Z_{Ni} - Z_{Fe})\,\xi = 2\xi$, will then give the "effective" number of electrons supplied by hydrogen to the conduction band of the metal. The existence of this similarity for Ni-Fe alloys with $x_{Fe} > 0.6$, which are weak itinerant ferromagnets (i.e. which have holes both in the $d\downarrow$- and $d\uparrow$-subbands at 0 K), is a strong argument in favour of the fact that in fairly wide ranges of concentration, the rigid band model is a good approximation for describing the magnetic properties of all fcc Ni-Fe alloys as well as the fact that the rigid d-band model can be used for hydrogen solutions based on these alloys.

4.4.2.2. Ni-Co-H system. In [4.40], we have investigated hydrogen solutions in fcc $Ni_{70}Co_{30}$ and $Ni_{40}Co_{60}$ alloys which are strong itinerant ferromagnets. As in strong itinerant Ni-Fe ferromagnets with $x_{Fe} \leqslant 0.6$, dissolution of hydrogen in these alloys decreases σ_0 and T_C. The linear approximation to the experimental σ_0 vs. n dependences for $n < 0.8$ gives slopes $\partial\sigma_0/\partial n = -0.76\mu_B$ and $-0.71\mu_B$ per H atom for the single-phase $Ni_{70}Co_{30}$-H and $Ni_{40}Co_{60}$-H solutions respectively, which agrees with the predictions of the rigid d-band model. An attempt to describe the σ_0 (n) and T_C (n) dependences for the Ni-Co alloys with the same coefficients of similarity ξ (introduced through relations analogous to (4.3)) did

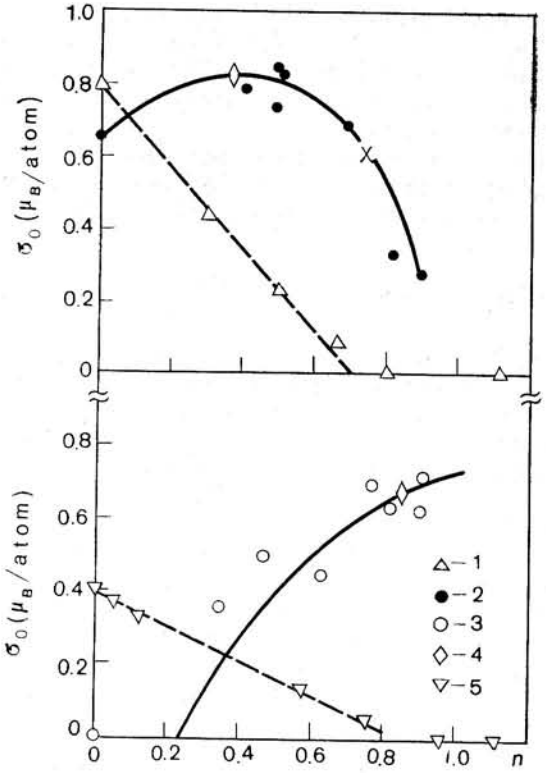

Fig. 4.21. Dependence of the spontaneous magnetization σ_0 at $T = 0$ K on the hydrogen concentration n in disordered Ni-Mn alloys [4.56] (*1*—10, *2*—20, *3*—30 At. % Mn; *4*—values of σ_0 used for calculating ξ), and in the $Ni_{95}Cr_5$ alloy (*5*—results of the present paper).

not lead to such a good agreement between the calculated and experimental values of $T_C(P_{H_2})$ as for the Ni-Fe alloys, but the sign and order of magnitude of the effect were found to be correct.

4.4.2.3. Ni-Mn-H system. The σ_0 vs. x_{Mn} dependence for disordered fcc Ni-Mn alloys is not monotonic (see Fig. 4.17). The spontaneous magnetization of nickel ($N^e = 10$ electrons per atom) is given by $\sigma_0^{Ni} \approx 0.616\ \mu_B$ per atom. Upon substituting manganese for nickel, σ_0 increases, attains its maximum value $\sigma_0^{max} \approx 0.8\mu_B$ per atom at $x_{Mn} \approx 0.1$, and then begins to decrease [4.66]. The Curie points decrease monotonically from 627 K for pure nickel to helium temperatures for the alloy with $x_{Mn} \approx 0.26$. The σ_0 (n) dependences obtained by us in [4.56] for hydrogen solutions in disordered Ni-Mn alloys with 10, 20, and 30 at. % Mn are shown in Fig. 4.21. Just as in the Ni-H system, a separation into γ_1- and γ_2-phases is observed

in the $Ni_{90}Mn_{10}$-H system at atmospheric pressure and $T \leqslant 150$ K. The γ_2-phase is paramagnetic at $T \geqslant 4.2$ K, and a nearly linear decrease in σ_0 in the range of hydrogen concentrations $0 \leqslant n \leqslant 0.7$ is caused by the decrease in the content of the ferromagnetic γ_1-phase in the two-phase mixture ($\gamma_1 + \gamma_2$) with increasing n. A separation of the $Ni_{80}Mn_{20}$-H and $Ni_{70}Mn_{30}$-H solutions into γ_1- and γ_2-phases was not observed.

The magnetization of the Ni-Mn-H solutions at room temperature was also investigated in [4.78] (for samples which were electrolytically saturated with hydrogen under atmospheric pressure) and in [4.79] directly under high hydrogen pressure. The results of these measurements are in accord with the data given in [4.56].

A comparison of Figs. 4.21 and 4.17 shows that as for Ni-Fe and Ni-Co alloys, the σ_0 (n) and σ_0 (Δx_{Mn}) dependences for Ni-Mn alloys are similar. Let us introduce the coefficients $\zeta = \Delta N^e/n$ relating the changes in composition and, correspondingly, electron concentration N^e in the initial alloys with the changes in n leading to identical changes in σ_0. A comparison of the values of σ_0 (n) for $Ni_{80}Mn_{20}$-H and $Ni_{70}Mn_{30}$-H solutions, shown in Fig. 4.21 by diamond-shaped symbols, with the values of σ_0 (x_{Mn}) presented in [4.66] for Ni-Mn alloys, gives $\zeta = 0.81$ and 0.48 electron per H atom, respectively. The σ_0 vs. n curves calculated for these values of ζ for the $Ni_{80}Mn_{20}$ and $Ni_{70}Mn_{30}$ alloys are shown in Fig. 4.21 by solid lines. It can be seen that they satisfactorily agree with the experimental σ_0 vs. n dependences.

Thus, the effect of dissolved hydrogen on σ_0 of Ni-Mn alloys is completely analogous to the effect of substituting nickel for manganese. There is no such analogy for the Curie points for alloys with 10 and 20 at. % Mn: an increase in the nickel content in Ni-Mn alloys increases T_C, while injection of hydrogen decreases T_C. The T_C vs. n and T_C vs. Δx_{Ni} dependences again become similar for the alloy with 30 at. % Mn: a saturation of this alloy with hydrogen up to $n = 0.85$ (the value of σ_0 for this composition of the solution is indicated by the diamond-shaped symbol in Fig. 4.21) leads to a monotonic increase in its Curie point to ~250 K, while for the $Ni_{83.5}Mn_{16.5}$ alloy (which has the same value of σ_0), $T_C \approx 400$ K [4.52].

4.4.2.4. Ni-Cr-H system. Summing up the results described in subsections 4.4.2.1-3, it can be stated that the σ_0 vs. n dependences for γ-solutions based on alloys of nickel with iron, cobalt, and manganese are analogues to the corresponding σ_0 vs. x_{Ni} dependences for the initial binary alloys. Such an analogy also holds for the Curie points, the only exception being Ni-Mn alloys with 10 and 20 at. % Mn. An entirely different behaviour of the magnetic properties was observed in the case of Ni-Cr alloys. A replacement of chromium by nickel in these alloys leads to the increase both in σ_0 (Fig. 4.17) and T_C

[4.52]. Our measurements have shown that an increase in the hydrogen concentration in the γ_1-phase of the $Ni_{95}Cr_5$-H solution results in a significant lowering of T_C (Fig. 4.15), while the γ_2-phase of this solution is paramagnetic at $T \geqslant 4.2$ K; see Fig. 4.21 (for $n \leqslant n_{\gamma_2}^{\min} \approx 0.8$, the samples consisted of a mixture of γ_1- and γ_2-phases; so, the magnetization of the samples was proportional to the content of the ferromagnetic γ_1-phase). A decrease in σ_0 and T_C for Ni-Cr alloys containing up to 7 at. % Cr was also observed upon electrolytic saturation by hydrogen [4.80].

4.4.2.5. Discussion of properties of Ni-Me-H solutions. Earlier, we discussed in detail one limiting case: hydrogen solutions in strong itinerant ferromagnets (Ni-Co and Ni-Fe with $x_{Fe} \leqslant 0.6$), when the concentration dependence of the magnetic properties of the initial alloys was mainly determined by the degree to which the *d*-band is filled and not by its deformation.

The other limiting case, when a change in the alloy composition strongly deforms the band structure, is realized, for example, for Ni-Cr and Ni-V alloys. In these alloys, the perturbing potential introduced by the Cr and V atoms is large enough to shift the virtual $d^5\uparrow$-levels of the impurity atoms above the Fermi level (see Fig. 4.18*c*). The electrons from these states go over into the conduction band, increasing the degree of filling of the *d*-states of nickel, which decreases T_C and σ_0. Upon hydrogenation of such alloys, the electrons supplied by the hydrogen atoms will also mainly fill the *d*-band of nickel in view of its high density of states at the Fermi level, thus decreasing T_C and σ_0. It is exactly this situation that is observed upon saturation of Ni-Cr alloys with hydrogen.

Thus, in both limiting cases, the band theory of ferromagnetism can explain the observed dependences $\sigma_0(n)$ and $T_C(n)$ under the assumption that it is the degree of filling of the *d*-band of the metal by electrons that has a dominating effect on the magnetic properties upon hydrogenation. The situation is more complicated in the case of alloys for which the σ_0 vs. N^e dependences deviate from the straight line with the slope $\partial\sigma_0/\partial N^e \approx -1\mu_B$ per electron only for a large impurity concentration. Such magnets include Ni-Fe alloys with $x_{Fe} > 0.6$ and Ni-Mn alloys with $x_{Mn} \geqslant 0.1$ (see Fig. 4.17). These itinerant ferromagnets are weak, i.e. at 0 K they have a considerable number of holes in the $d\downarrow$- as well as $d\uparrow$-subband. The role of band structure deformation in the $\sigma_0(x_{Ni})$ dependences for these alloys is at present the subject of controversy, especially for the Ni-Fe alloys which exhibit anomalous physical properties (Invar nature) in this concentration range. Here the converse is true: the observed analogy in the behaviour of σ_0 (and of T_C in most cases) with increasing Ni concentration and with hydrogenation indicates that the magnetic properties of the initial alloys (without hydrogen) are to be mainly determined by the degree of filling of the *d*-band rather than its deformation, over a fairly wide range of concentrations ($\Delta N^e \leqslant \zeta\, n \leqslant 0.5$ electron per atom). Indeed, let us assume that for values of N^e smaller than a certain limiting value N^e_{lim}, the deviations from the straight line

$$\sigma_0(N^e) \approx \sigma_0^{Ni} + (N^e - N^e_{Ni})\,\mu_B \qquad (4.6)$$

(which describes the behaviour of spontaneous magnetization of strong itinerant ferromagnets with an fcc lattice) in Ni-Fe and Ni-Mn alloys are caused by sharp (taking place in the interval $\Delta N^e \ll 0.5$ electron per atom) and qualitatively different changes in the band structure. Experiments show that for both groups of alloys, the effect of hydrogen on σ_0 of alloys with $N^e < N^e_{lim}$ is completely equivalent to the effect of increasing their electron concentration. This equivalence is illustrated especially clearly by the coincidence of the maximum values σ_0^{max} in the σ_0 vs. *n* dependences for the solutions $Ni_{32.5}Fe_{67.5}$-H (Fig. 4.19, $\sigma_0^{max} \approx 1.85\mu_B$ per atom) and $Ni_{80}Mn_{20}$-H (Fig. 4.21, $\sigma_0^{max} \approx 0.8\mu_B$ per atom) with the maximum values in the corresponding σ_0 vs. N^e dependences for Ni-Fe and Ni-Mn alloys (Fig. 4.17). Consequently, the effect of hydrogen on the band structure of Ni-Fe alloys is opposite to the effect of substituting Fe for Ni in Ni-Fe alloys and Mn for Ni in Ni-Mn alloys. In other words, according to our starting assumption, these two effects are qualitatively different. This, however, is extremely unlikely: the entire body of the experimental and theoretical data shows that hydrogen must slightly deform the *d*-band of the metals and should only increase the degree of filling of this band by electrons.

Thus, the analysis of the effect of hydrogen on the magnetic properties of the Ni-Fe and Ni-Mn alloys leads to the conclusion that the deviation of the dependences for these alloys from (4.6) is due not to a sharp change in the *d*-band structure or in the nature of the exchange interaction in the region of the "anomalous" behaviour of the σ_0 vs. N^e dependences, but at the very least due to the changes gradually accumulating over a wide concentration range of the order of the total content of Fe and Mn in the alloys. It should be noted that the concentration dependence of these changes is much weaker when nickel is alloyed with iron (in this case, a value $\Delta N^e = (Z_{Ni} - Z_{Fe})\,x_{Fe} \approx 2.0 \times 0.6 = 1.2$ electron per atom is required for the σ_0 vs. N^e dependence to begin deviating from (4.6)) than in the case of alloying with manganese (here, ΔN^e is equal to $3 \times 0.1 = 0.3$ electron per atom). Probably, the stronger deformation of the band structure of nickel when it is alloyed with manganese rather than iron is responsible for the fact that, in contrast to all the investigated Ni-Fe alloys, no analogy is observed for Ni-Mn alloys with 10 and 20 at. % Mn in the change of the Curie points with the alloy composition and with saturation by hydrogen.

4.4.3. $Fe_{65}(Ni_{1-x}Mn_x)_{35}$-H Solutions

The $Fe_{65}(Ni_{1-x}Mn_x)_{35}$ alloys (percent by weight) are a classical system which has served for many years as a model for investigating the problems of the competition between ferromagnetic and antiferromagnetic ordering in fcc metals. These alloys provided a rare opportunity to systematically observe the effect of hydrogen on both types of magnetic ordering for the same group of objects.

The substitution of Mn for Ni in the $Fe_{65}(Ni_{1-x}Mn_x)_{35}$ system decreases the Curie temperature from $T_C = 467$ K for the $Fe_{65}Ni_{35}$ alloy to helium temperatures for the alloy containing ~10% Mn. For higher manganese concentrations, antiferromagnetic ordering takes place in the system, and the Néel temperature increases monotonically up to $T_N = 442$ K for the $Fe_{65}Mn_{35}$ alloy. Both ferromagnetically and antiferromagnetically ordered alloys exhibit anomalous physical properties characteristic of Invars (see [4.81, 82]).

Using the technique developed by the authors for compressing hydrogen to 7 GPa, γ-solutions with concentrations up to $n \sim 1$ were obtained for alloys over the entire concentration range from $Fe_{65}Ni_{35}$ to $Fe_{65}Mn_{35}$ [4.83]. The σ_0 vs. n and T_C vs. n dependences for the Fe-Ni-Mn-H solutions are shown in Fig. 4.22. The following is observed when the $Fe_{65}(Ni_{1-x}Mn_x)_{35}$ alloys are saturated with hydrogen. The Néel temperatures of the antiferromagnetic alloys decrease, and a ferromagnetic ordering sets in for a certain concentrations n_f of hydrogen. After this, the Curie temperatures of the ferromagnetic solutions increase monotonically. Therefore, the change in the magnetic properties of the $Fe_{65}(Ni_{1-x}Mn_x)_{35}$ alloys as a result of hydrogenation turned out to be analogous to their change upon substituting Ni for Mn (which increases the electron concentration N^e). As shown in [4.84], the shape of the Mössbauer spectrum of hydrogen-saturated alloy $Fe_{66}Ni_{31}Mn_3$ (atomic percent) also approaches the shape of the spectrum for the $Fe_{65}Ni_{35}$ alloy.

Let us introduce the similarity coefficients ζ for the dependences of the magnetic properties of the alloys with and without hydrogen. If we assume that the concentration dependence of the magnetic properties of the pseudo-binary $Fe_{65}(Ni_{1-x}Mn_x)_{35}$ system, as well as the dependence of these properties on the hydrogen content of these alloys, is mainly determined by the change in the degree of filling of the d-band, then for all these alloys and hydrogen solutions based on them, one and the same effective concentration N_f^e of electrons should exist, at which ferromagnetic ordering sets in. Assuming that the values of ζ do not differ much for the investigated alloys, we get $\langle\zeta\rangle = 0.7$ electron per H atom and $N_f^e = 8.35$ electrons per atom from the equation

$$N^e + \langle\zeta\rangle n_f = N_f^e$$

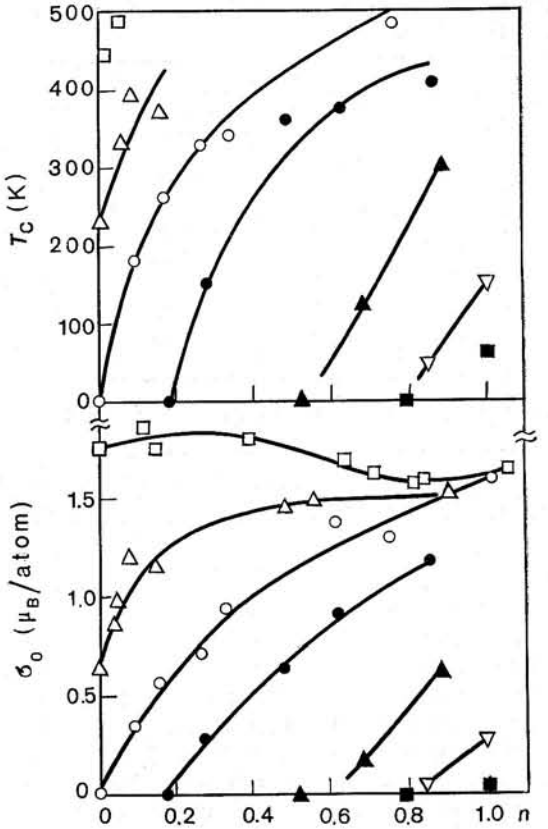

Fig. 4.22. T_C vs. n and σ_0 vs. n dependences for hydrogen solutions in fcc alloys $Fe_{65}(Ni_{1-x}Mn_x)_{35}$ [4.83]. The notation is the same as in Fig. 4.23.

by using the method of least squares and the values of N^e and n_f given in Table 4.2. The values of $N_f^e - N^e$ and $\zeta = (N_f^e - N^e)/n_f$ are also given in this table. It is seen that the sign and the order of magnitude of the ζ's obtained in this way are in agreement with the assumption that the degree of filling of the d-band plays a dominating role in the formation of the dependences of the magnetic properties of the investigated alloys on nickel and hydrogen concentration.

The results of investigations of hydrogen solutions in $Fe_{65}(Ni_{1-x}Mn_x)_{35}$ alloys not only confirm the earlier notions about the nature of the influence of hydrogen on the magnetic properties of transition metals, but also reveals new aspects of this influence. As a matter of fact, the magnetic properties of the $Fe_{65}(Ni_{1-x}Mn_x)_{35}$ alloys [4.81, 82] and hydrogen solutions based on them [4.83] are

Table 4.2. Parameters for Hydrogen Solutions in $Fe_{65}(Ni_{1-x}Mn_x)_{35}$ Alloys [4.83]

Mn wt.%	T_C, K	T_N, K	N^e el/atom	$N_f^e - N^e$ el/atom	n_f	ζ el/atom
0	467	—	8.68	−0.33	—	—
4.5	228	—	8.54	−0.19	—	—
10	—	—	8.38	−0.03	0	—
17	—	160	8.17	0.18	0.18	1.00
24	—	253	7.97	0.38	0.58	0.66
29	—	341	7.82	0.53	0.81	0.65
35	—	442	7.62	0.70	0.94	0.74

Remark: $\zeta = (N_f^e - N^e)/n_f$; $N_f^e = 8.35$ el/atom in the Fe-Ni-Mn alloy.

well described by the equations of the theory of very weak itinerant ferromagnetism [4.85]. In particular, it follows from these equations that

$$\frac{T_C}{\sigma_0} = \frac{1}{2\pi k_B \mathscr{N}(\mathscr{E}_F)} \left[\frac{3\nu_1^2 - \nu_2}{\nu_1^2 - \nu_2} \right]^{1/2} \tag{4.7}$$

for weak itinerant ferromagnets (k_B is the Boltzmann constant, $\mathscr{N}(\mathscr{E}_F)$ is the density of states at the paramagnetic Fermi level $\mathscr{E}_F$, while $\nu_m = \mathscr{N}^{(m)}(\mathscr{E}_F)/\mathscr{N}(\mathscr{E}_F)$). In fcc ferromagnets, the Fermi level seems to pass near the maximum of the density of states curve $\mathscr{N}(\mathscr{E})$ [4.66], which gives $\nu_2 \leqslant 0$. For $\nu_2 \leqslant 0$, the values of the factor in square brackets in Eq. (4.7) depend slightly on the magnitudes of the parameters entering into it, changing from 3 for $\nu_2 = 0$ to 1 for $\nu_2 \to -\infty$. For a parabolic band, this factor is equal to 2. Thus, the density of states at the paramagnetic Fermi level for a weak itinerant ferromagnet can be roughly estimated if T_C and σ_0 are known:

$$\frac{T_C}{\sigma_0} \approx \frac{1}{\sqrt{2}\,\pi k_B \mathscr{N}(\mathscr{E}_F)}. \tag{4.8}$$

The T_C vs. σ_0 dependence for the $Fe_{65}(Ni_{1-x}Mn_x)_{35}$ system is shown in Fig. 4.23. It can be seen that for the investigated samples, the values of T_C as a function of σ_0 lie nearly on a single curve (in order to show how strongly the T_C vs. σ_0 dependences can deviate from one another for different itinerant ferromagnets, the point for Ni is indicated in Fig. 4.23 by the diamond-shaped symbol). It follows from Eq. (4.8) that a common dependence of T_C on σ_0 for all Fe-Ni-Mn alloys and hydrogen solutions based on them is indicative of a unique relation between the values of T_C and σ_0 for these materials and $\mathscr{N}(\mathscr{E}_F)$ at the paramagnetic Fermi level.

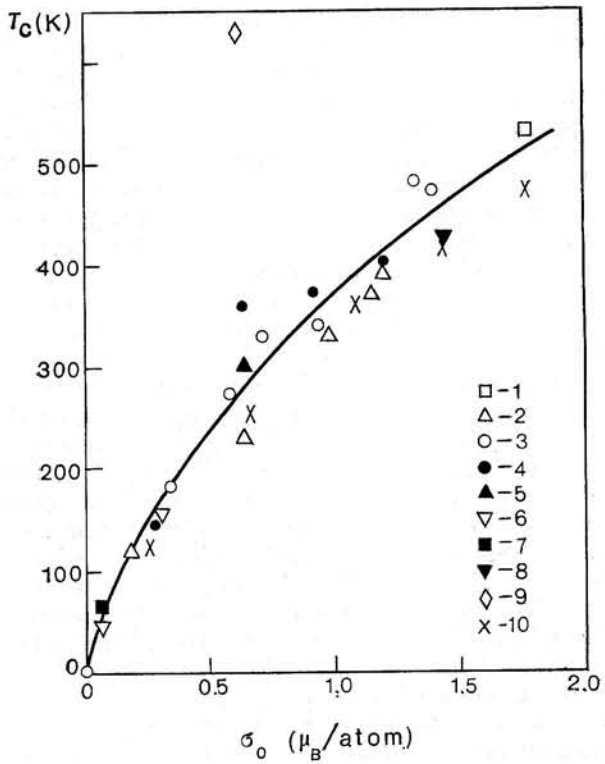

Fig. 4.23. Dependence of Curie points T_C on spontaneous magnetization at $T = 0$ K.
1-7—γ-solutions of hydrogen in the alloys $Fe_{65}(Ni_{1-x}Mn_x)_{35}$ [4.83] (*1*—0; *2*—4.5; *3*—10; *4*—17; *5*—24; *6*—29; *7*—35 wt. % Mn); *8*—Ni-Fe alloy containing 67.5 at. % Fe [4.58, 87]; *9*—nickel; *10*—$Fe_{65}(Ni_{1-x}Mn_x)_{35}$ alloys [4.81].

This result correlates well with all the facts indicating a weak deformation of *d*-bands and small changes in the dependences of the exchange interaction as a function of the degree of filling of the *d*-band, accompanying hydrogenation of fcc nickel alloys, including the Ni-Fe Invars. Indeed, if the possibility of random coincidences is neglected, several conditions must be satisfied simultaneously in order that the weak itinerant ferromagnets with the same density of states $\mathscr{N}(\mathscr{E}_F)$ at the paramagnetic Fermi level have the same Curie temperatures and the same values of spontaneous magnetization over a wide range of values of $\mathscr{N}(\mathscr{E}_F)$. Firstly, the form of the *d*-band must be the same for all these ferromagnets. Secondly, the degree of filling of their *d*-bands must be the same. Finally, the relative shift of the $d\uparrow$- and $d\downarrow$-subbands, $\Delta = I\sigma$, must also be the same at all

temperatures, i.e. the effective exchange interaction parameters I must be equal. Hence, the data for the $Fe_{65}(Ni_{1-x}Mn_x)_{35}$ alloys shown in Fig. 4.23 indicate that the change in the magnetic properties upon substituting nickel for manganese in this pseudo-binary system, as well as upon a saturation of these alloys by hydrogen, is mainly due to the increase in the degree of filling of the d-band and, in addition, the phenomenological coefficients $\zeta < 1$ electron per H atom for the Fe-Ni-Mn-H solutions are close to the number η of electrons supplied by the hydrogen atoms above the Fermi level.

Such conclusions also provide a certain clarification for one of the most complicated questions arising in the discussion of the influence of hydrogen on the magnetic properties of transition metals, namely, the role of volume effects: the $Fe_{65}(Ni_{1-x}Mn_x)_{35}$ alloys, just as the Ni-Fe alloys with $x_{Fe} \geqslant 0.6$, are Invars whose characteristic feature is a strong dependence of the magnetic properties on volume.

The solid line in Fig. 4.24 shows the σ_0 vs. N^e dependence for fcc Ni-Fe alloys under atmospheric pressure. The dotted lines show the analogous dependences for $P = -5$ and $+5$ GPa, calculated by assuming that σ_0 depends linearly on volume and by using the experimental values of $(1/\sigma_0)\,(\partial\sigma_0/\partial P)_{1n}$ obtained under hydrostatic compression [4.46, 86]. For $N^e \leqslant 9$ electrons per atom, the slope of the σ_0 vs. N^e dependence for $P = -5$ GPa increases sharply. For example, when N^e decreases from 8.9 to 8.7 electrons per atom, σ_0 increases by $\sim 0.9\mu_B$ per atom. If the itinerant ferromagnet is strong [and the number of holes in the d-bands of nickel-based fcc alloys is such that these alloys must become strong ferromagnets when the magnetization attains the value $\sigma_0\,(N^e) \sim \sigma_0^{Ni} + (N^e - 10)\,\mu_B$], a change in the degree of filling of the d-band by $\Delta N^e = 8.9 - 8.7 = 0.2$ electron per atom increases σ_0 by only $\sim 0.2\mu_B$ per atom. The increase in σ_0 by the remaining amount $\sim (0.9 - 0.2) = 0.7\mu_B$ per atom can take place only as a result of an additional decrease in the number of electrons in the d-band due to another mechanism, for example, on account of a transfer of ~ 0.7 electron per atom to the s-band. This is unlikely, since this number of electrons is comparable to the total number of occupied states in the s-band.

Thus, in order for the σ_0 vs. N^e dependence at $P = -5$ GPa shown in Fig. 4.24 to be realized, this pressure must lead to catastrophic changes in the band structure (and exchange interaction) in Invar alloys. The dissolution of $n \sim 1$ of hydrogen in such alloys causes an increase in the volume that is equivalent to the action of a negative pressure ~ 15 GPa and, at the same time, as we have seen, it slightly changes the shape of the d-band and the dependence of the exchange interaction parameter on the degree of filling of the band. It should be recalled that hydrogenation of the Ni-Fe Invars with 66.1 and 67.5 % Fe does not increase their spontaneous magnetization beyond the value $\sigma_0^{max} \approx 1.9\mu_B$ per atom, the maximum value for Ni-Fe alloys without hydrogen (see Fig. 4.19). Since the compression of Invars leads to a sharp decrease in σ_0 (see Fig. 4.24, curve 2), this suggests that the σ_0 vs. V dependence is asymmetric with respect to the volume V_0 under atmospheric pressure: for $V < V_0$, the magnetization increases with increasing V, while for $V \sim V_0$, it reaches a stationary value and subsequently remains practically unchanged.

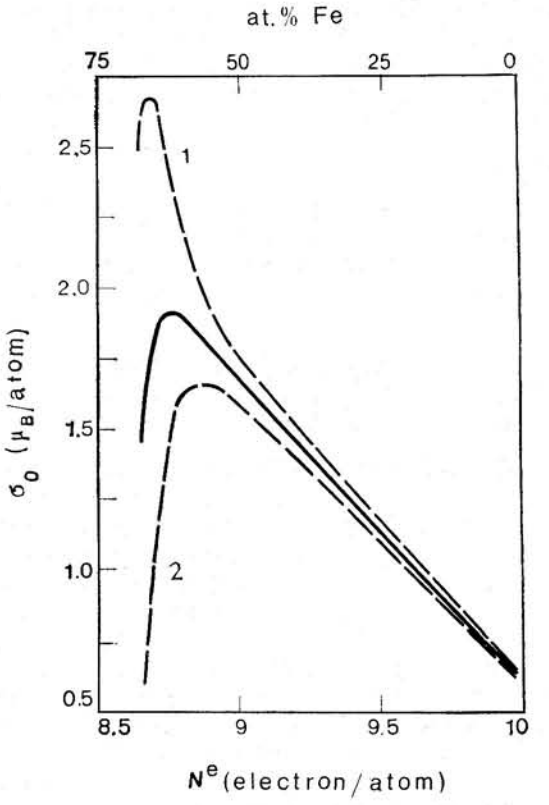

Fig. 4.24. Concentration dependences of σ_0 or Ni-Fe alloys. The solid line shows the curve obtained under atmospheric pressure [4.65, 66]; *1* and *2* represent the curves for $P = -5$ and $+5$ GPa, respectively.

It is interesting that in contrast to the σ_0 vs. n dependences, the T_C vs. n dependences for the investigated Ni-Fe alloys can be explained by considering the increase in volume during hydrogenation to be the main effect and by using the T_C vs. V dependences obtained under conditions of compression [4.87, 58]. However, such facts

like the possibility of describing the T_C vs. n dependence within the scope of the rigid d-band model with reasonable values of η, and unduly high estimates for values of σ_0 for hydrogen solutions in Invar alloys while taking into account the volume effects (using the values of $\partial\sigma_0/\partial V$ obtained under compression), cast doubts over the physical content of estimates of the effect of variations of volume on the Curie temperatures as well.

Summing up the above presentation, it can be stated that the problem of the role of volume effects in the change in the magnetic properties of transition metals upon hydrogenation is nontrivial and is an interesting field for further research.

4.4.4. Applicability of the Rigid d-band Model for Describing the Magnetic Properties for Other Me-H Solutions

4.4.4.1. Hydrogen solutions in fcc alloys based on 3d-metals. The concept of hydrogen as a donor of a fractional number of electrons in a weakly deformed d-band of the host metal, which is one of the most significant results of the investigations of magnetic properties of γ-solutions Ni-Me-H, allows at least a qualitative prediction of the behaviour of these properties for a number of systems. For example, an increase in n should lower σ_0 and T_C of strong itinerant ferromagnets (Ni-Cu, Ni-Zn, Co-Fe; for Ni-Cu alloys, this fact is confirmed experimentally, see [4.88, 89]) and alloys for which $\partial\sigma_0/\partial N^e > 0$ for low impurity concentrations (Ni-V, Co-Mn, Co-Cr). Owing to the high density of states at the Fermi level of nickel and cobalt, the electrons of the dissolving hydrogen must fill the d-band in fcc alloys of these metals with nontransition elements (Ni-Al, Ni-Ge, Co-Sb, etc.) as well, again lowering σ_0 and T_C. An increase in σ_0 with hydrogen concentration should apparently be observed only for those alloys with $\partial\sigma_0/\partial N^e > 0$, for which the σ_0 vs. N^e dependences deviate from (4.6) only for a large impurity concentration, i.e. this deviation is to a large extent due to the degree of filling of the d-band (Ni-Fe alloys with $x_{Fe} > 0.6$ and Ni-Mn alloys with $x_{Mn} > 0.1$).

4.4.4.2. Hydrogen solutions in 3d-metals with hcp lattice. A necessary condition for using the rigid d-band model to describe the magnetic properties of Me-H solutions is a knowledge of the dependence of these properties on the occupancy of the d-band in the starting materials (without hydrogen). For fcc metals, such information can be obtained, for example, from the σ_0 (N^e) and T_C (N^e) dependences for alloys of 3d-metals closely positioned in the Periodic Table, whose properties are described well by the rigid band model. The concentration dependences of the magnetic properties of alloys with an hcp lattice have been investigated to a much lesser extent,

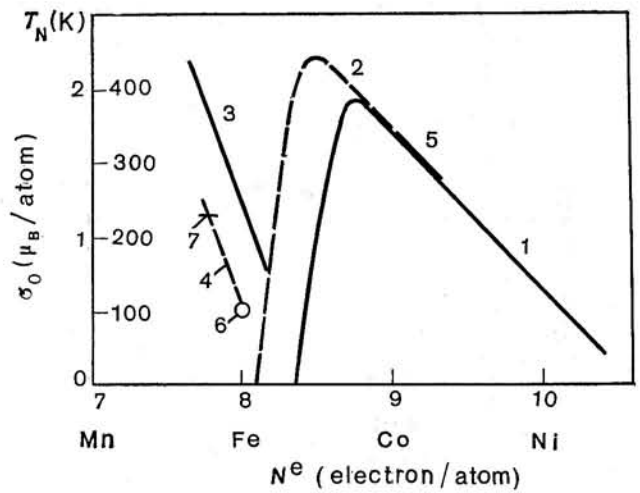

Fig. 4.25. Concentration dependences of spontaneous magnetization σ_0 at $T = 0$ K and of Néel temperatures T_N for the alloys of 3d-metals that are nearest neighbours in the periodic table.
γ—fcc alloys; ε—hcp alloys. *1*—σ_0^γ; *2*—σ_0^ε; *3*—T_N^γ; *4*—T_N^ε; *5*—σ_0^ε for Co-Ni alloys; *6*—T_N^ε for Fe; *7*—T_N^ε for Fe-Mn alloys.

primarily due to relatively narrow intervals of the mutual solubility of 3d-metals in hexagonal phases. However, for $N^e \geqslant 7.7$ electrons per atom, these dependences are apparently similar for hcp and fcc alloys.

Indeed, for fcc alloys of 3d-metals closely positioned in the Periodic Table, the values of σ_0 as a function of N^e lie on a single curve (see Fig. 4.25). With decreasing N^e to ~8.8 electrons per atom, σ_0 increases almost linearly with a slope $\partial\sigma_0/\partial N^e \approx -\mu_B$ per electron (Ni-Cu, Ni-Co, and Ni-Fe alloys), reaches a maximum, and then begins to decrease. For $N^e \approx 8.35$ electrons per atom, the alloys become paramagnetic down to helium temperatures. Then antiferromagnetic ordering sets in, and the Néel temperature monotonically increases up to $T_N \approx 440$ K at $N^e = 7.65$ electrons per atom (Fe_{65} $(Ni_{1-x}Mn_x)_{35}$ alloys).

As regards the magnetic properties of hcp metals and alloys, it is known that the σ_0 vs. N^e dependence for hcp Co-Ni alloys is nearly linear (segment of the solid line in Fig. 4.25), has a slope $\partial\sigma_0/\partial N^e \approx -\mu_B$ per electron and is close to the σ_0 vs. N^e dependence for fcc alloys [4.90, 91] (the slope $\partial\sigma_0/\partial N^e \approx -\mu_B$ per electron indicates that like the fcc alloys in the same interval of values of N^e, the hcp Co-Ni alloys are strong itinerant ferromagnets). Extrapolation from the Fe-Ru and Fe-Os alloys [4.92] shows that the

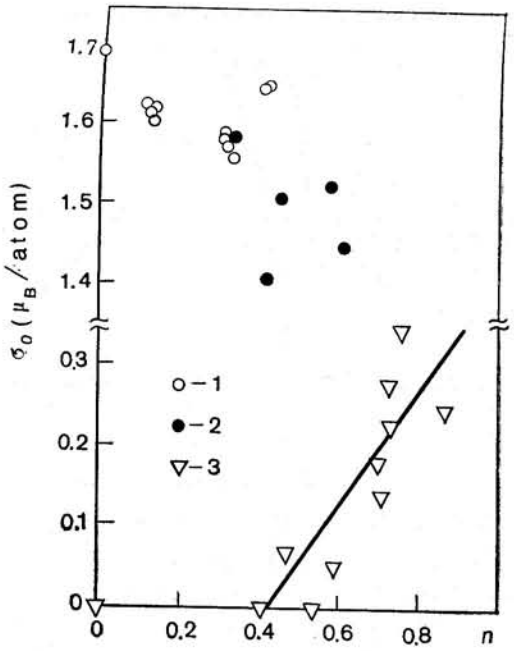

Fig. 4.26. σ_0 vs. n dependence for ε-solutions Co-H (*1*—results of [4.64]; *2*—results of the present paper), and $Fe_{77.6}Mn_{22.4}$-H (*3*—results of [4.94]).

virtual hcp phase of iron ($N^e = 8$ electrons per atom) is an antiferromagnet with $T_N \approx 100$ K (the circle in Fig. 4.25). The hcp Fe-Mn alloys ($7.71 \leqslant N^e \leqslant 7.82$ electrons per atom) are antiferromagnets with $T_N \approx 230$ K [4.93] (the horizontal segment of the solid line in Fig. 4.25). Sufficiently correct data on the magnetic properties of hcp alloys with $8 < N^e < 9$ electrons per atom are unavailable in the literature. One can, however, expect that in this range of electron concentration as well, the σ_0 vs. N^e and T_N vs. N^e dependences for hcp alloys are similar to those for fcc alloys (the dotted line in Fig. 4.25).

As is seen from the above, the objects of interest to us from the point of view of investigating the effect of hydrogen on the magnetic properties of hcp alloys are basically exhausted by cobalt, iron, and Fe-Mn alloys in which the hcp phase is metastable at atmospheric pressure in the concentration range between 18 and 30 at. % Mn [4.52]. The results of investigations of the σ_0 vs. n dependence for the ε-solutions Co-H are shown in Fig. 4.26. The experimental data show a considerable spread in values, but the general tendency is a lowering of spontaneous magnetization with increasing hydrogen

concentration (at present, we are engaged in a more accurate determination of the σ_0 vs. n dependence for the ε-solutions Co-H and the investigation of magnetic properties of the γ-solutions). This is exactly how σ_0 should behave upon hydrogenation of a strong itinerant ferromagnet according to the rigid d-band model.

If the rigid d-band model is also valid for the ε-solutions of hydrogen in iron and Fe-Mn alloys, and if our conjectures concerning the dependence of magnetic properties of these materials on the degree of filling of the d-band (Fig. 4.25) are true, the dissolution of hydrogen must convert them from antiferromagnets to ferromagnets. Experiments have shown that this is actually the case. The ε-solution Fe-H for $n \approx 0.8$ was found to be a ferromagnet with $\sigma_0 \approx 2.2\mu_B$ per Fe atom [4.37]. At $n \gtrsim 0.4$, the appearance of spontaneous magnetization was observed for $Fe_{77.6}Mn_{22.4}$-H as well [4.94] (the σ_0 vs. n dependence for these solutions is shown in Fig. 4.26; the investigated samples were single-phase materials).

It is interesting to note that the results of investigations of Fe-H and Fe-Mn-H ε-solutions, confirming the identical character of the σ_0 vs. N^e dependences for hcp and fcc alloys of 3d-metals with $N^e \gtrsim 8$ electrons per atom on the whole, reveal, at the same time, a certain difference between them (like the one shown in Fig. 4.25). Indeed, according to the rigid d-band model, the value of $\sigma_0 \approx \approx 2.2\mu_B$ per Fe atom for the ε-hydride of iron cannot, as a function of the effective electron concentration $N^e + \eta n$, lie above the continuation of the σ_0 (N^e) straight line for hcp Co-Ni alloys, since for the alloys having values of σ_0 lying on this straight line, the holes must be only in the $d\downarrow$-subband, and hence the magnetization has its maximum possible value for the given degree of filling of the d-band. As is easily seen from Fig. 4.25, the maximum of the σ_0 vs. N^e dependence for hcp alloys shifts noticeably due to these restrictions to the left along the N^e-axis with respect to its position on the dependence for fcc alloys (for the ε-solutions Fe-H, such restrictions lead to the condition $\zeta \leqslant 0.6$ electron per H atom, which is a reasonable estimate [4.37]). Further, for the ε-solutions $Fe_{77.6}Mn_{22.4}$-H, ferromagnetism appears for $n \approx 0.4$. Even if we assume that $\eta = 1$ electron per H atom for the $Fe_{77.6}Mn_{22.4}$ alloy (the value of η for the Me-H solutions investigated to date is found to be lower), the appearance of ferromagnetism in hydrogen solutions on its base will correspond to the effective electron concentration $N^e + \eta n \approx \approx 7.8 + 0.4 = 8.2$ electrons per atom, which is less than the electron concentration $N^e \approx 8.35$ electrons per atom corresponding to the appearance of ferromagnetic ordering in fcc alloys.

Thus, under the above assumptions, we get a consistent picture describing unambiguously all the available data on concentration dependence of the magnetic properties of 3d-metals with an hcp lattice and their alloys as well as hydrogen ε-solutions based on them.

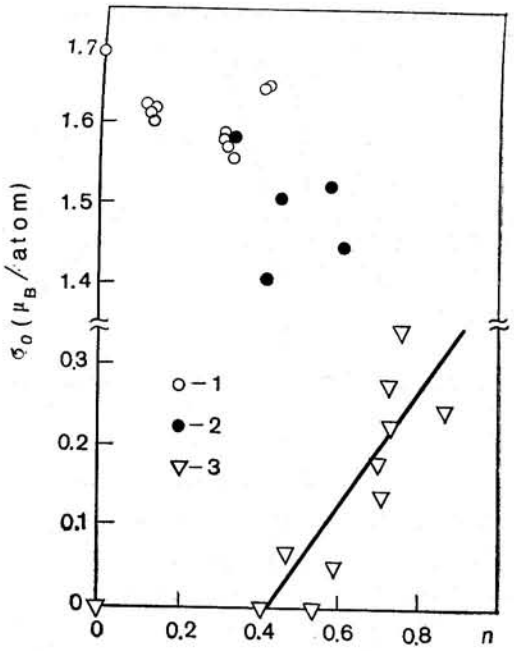

Fig. 4.26. σ_0 vs. n dependence for ε-solutions Co-H (*1*—results of [4.64]; *2*—results of the present paper), and $Fe_{77.6}Mn_{22.4}$-H (*3*—results of [4.94]).

virtual hcp phase of iron ($N^e = 8$ electrons per atom) is an antiferromagnet with $T_N \approx 100$ K (the circle in Fig. 4.25). The hcp Fe-Mn alloys ($7.71 \leqslant N^e \leqslant 7.82$ electrons per atom) are antiferromagnets with $T_N \approx 230$ K [4.93] (the horizontal segment of the solid line in Fig. 4.25). Sufficiently correct data on the magnetic properties of hcp alloys with $8 < N^e < 9$ electrons per atom are unavailable in the literature. One can, however, expect that in this range of electron concentration as well, the σ_0 vs. N^e and T_N vs. N^e dependences for hcp alloys are similar to those for fcc alloys (the dotted line in Fig. 4.25).

As is seen from the above, the objects of interest to us from the point of view of investigating the effect of hydrogen on the magnetic properties of hcp alloys are basically exhausted by cobalt, iron, and Fe-Mn alloys in which the hcp phase is metastable at atmospheric pressure in the concentration range between 18 and 30 at. % Mn [4.52]. The results of investigations of the σ_0 vs. n dependence for the ε-solutions Co-H are shown in Fig. 4.26. The experimental data show a considerable spread in values, but the general tendency is a lowering of spontaneous magnetization with increasing hydrogen

concentration (at present, we are engaged in a more accurate determination of the σ_0 vs. n dependence for the ε-solutions Co-H and the investigation of magnetic properties of the γ-solutions). This is exactly how σ_0 should behave upon hydrogenation of a strong itinerant ferromagnet according to the rigid d-band model.

If the rigid d-band model is also valid for the ε-solutions of hydrogen in iron and Fe-Mn alloys, and if our conjectures concerning the dependence of magnetic properties of these materials on the degree of filling of the d-band (Fig. 4.25) are true, the dissolution of hydrogen must convert them from antiferromagnets to ferromagnets. Experiments have shown that this is actually the case. The ε-solution Fe-H for $n \approx 0.8$ was found to be a ferromagnet with $\sigma_0 \approx 2.2\mu_B$ per Fe atom [4.37]. At $n \gtrsim 0.4$, the appearance of spontaneous magnetization was observed for $Fe_{77.6}Mn_{22.4}$-H as well [4.94] (the σ_0 vs. n dependence for these solutions is shown in Fig. 4.26; the investigated samples were single-phase materials).

It is interesting to note that the results of investigations of Fe-H and Fe-Mn-H ε-solutions, confirming the identical character of the σ_0 vs. N^e dependences for hcp and fcc alloys of 3d-metals with $N^e \gtrsim 8$ electrons per atom on the whole, reveal, at the same time, a certain difference between them (like the one shown in Fig. 4.25). Indeed, according to the rigid d-band model, the value of $\sigma_0 \approx \approx 2.2\mu_B$ per Fe atom for the ε-hydride of iron cannot, as a function of the effective electron concentration $N^e + \eta n$, lie above the continuation of the σ_0 (N^e) straight line for hcp Co-Ni alloys, since for the alloys having values of σ_0 lying on this straight line, the holes must be only in the $d\downarrow$-subband, and hence the magnetization has its maximum possible value for the given degree of filling of the d-band. As is easily seen from Fig. 4.25, the maximum of the σ_0 vs. N^e dependence for hcp alloys shifts noticeably due to these restrictions to the left along the N^e-axis with respect to its position on the dependence for fcc alloys (for the ε-solutions Fe-H, such restrictions lead to the condition $\zeta \leqslant 0.6$ electron per H atom, which is a reasonable estimate [4.37]). Further, for the ε-solutions $Fe_{77.6}Mn_{22.4}$-H, ferromagnetism appears for $n \approx 0.4$. Even if we assume that $\eta = 1$ electron per H atom for the $Fe_{77.6}Mn_{22.4}$ alloy (the value of η for the Me-H solutions investigated to date is found to be lower), the appearance of ferromagnetism in hydrogen solutions on its base will correspond to the effective electron concentration $N^e + \eta n \approx \approx 7.8 + 0.4 = 8.2$ electrons per atom, which is less than the electron concentration $N^e \approx 8.35$ electrons per atom corresponding to the appearance of ferromagnetic ordering in fcc alloys.

Thus, under the above assumptions, we get a consistent picture describing unambiguously all the available data on concentration dependence of the magnetic properties of 3d-metals with an hcp lattice and their alloys as well as hydrogen ε-solutions based on them.

It should, however, be emphasized that the applicability of the proposed model is, for the time being, limited to metals and alloys whose electron concentration lies in the interval $7.7 \leqslant N^e \leqslant 9.3$ electrons per atom. Beyond this interval, certain effects which cannot be explained within the scope of the model could be observed. The spontaneous magnetization observed for the ε-solutions Mn-H [4.27] may serve as an example of this kind. The nature of magnetism in these solutions is not clear so far and requires further investigations.

4.4.4.3. Hydrogen solutions in 4*d*-metal alloys. In contrast to metals at the end of the 3*d*-series, 4*d*-metals do not have properties which are simply and uniquely related to the degree of filling of the *d*-band, which makes if difficult to study experimentally the problem of the status of hydrogen in solutions based on them. It can, however, be stated that all available experimental data on the effect of hydrogen on the physical properties of these metals and their alloys (electron heat capacity, magnetic susceptibility, shape of the Mössbauer spectra, etc.) can be consistently explained by treating hydrogen as a donor contributing ~1 electron per H atom to the weakly deformed conduction band of the metal-solvent. A detailed discussion of these problems and references to the original papers are given, for example, in [4.72, 76, 11, 95].

4.5. Pd-Me-H SYSTEMS. SUPERCONDUCTIVITY AND PHASE TRANSFORMATIONS AT HIGH PRESSURE

Soon after the discovery of superconductivity in the Pd-H solutions with $n \geqslant 0.8$ [4.50], Stritzker [4.96] discovered that implantation of hydrogen in alloys of palladium with noble metals (Cu, Ag, and Au) may make them superconductors with critical temperature T_c up to 13-17 K, which is much higher than $T_c \approx 9$ K attained for the Pd-H solutions [4.51]. Stritzker's discovery provided a strong impetus for the development of experimental and theoretical investigations of superconducting properties of hydrogen solutions in alloys of palladium with various metals (a review and analysis of the most significant results of these investigations are given in [4.51]). It should, however, be noted that most of the experimental results on the superconductivity of Pd-Me-H solutions were obtained on samples which were saturated with hydrogen under nonequilibrium conditions (mainly through implantation), since the equilibrium solubility of hydrogen in the investigated alloys is not sufficiently high at pressures usually employed for hydrogenation. Samples obtained by implantation have rather peculiar properties: hydrogen is contained only in a narrow layer and is

distributed nonuniformly along its thickness, the metal lattice is known to be seriously damaged during implantation, and so on.

Using the technique for compressing hydrogen to high pressures, we were able to synthesize (under near-equilibrium conditions) macroscopic hydrogen-saturated samples of several palladium alloys. We began our investigations with hydrogen solutions in the alloys of palladium with Cu, Ag, Au, Ni, and Pt, which, according to the available data [4.51], possess the most interesting superconducting properties. Already the first experiments on the palladium-noble metal-hydrogen solutions have shown that the superconducting properties of homogeneous massive samples may radically differ from those of the samples obtained by hydrogen implantation.

The following is observed during implantation of hydrogen into the Pd-Cu, Pd-Ag, and Pd-Au alloys [4.96]. For a certain irradiation dose, the thin (~1500 Å) hydrogen-containing layer formed in the metal becomes superconducting. With further irradiation, T_c increases, reaches a maximum value T_c^m, and then begins to decrease. In its turn, the dependence of T_c^m on the concentration of the alloying element in palladium for each of the binary systems Pd-Cu, Pd-Ag, Pd-Au is also a curve with a maximum, the maximum values being $T_c^{mm} \approx 16.6$, 15.6, and 13.6 K respectively, for the $Pd_{55}Cu_{45}$, $Pd_{70}Ag_{30}$ and $Pd_{84}Au_{16}$ alloys. The typical T_c vs. n dependence upon hydrogen implantation in the $Pd_{55}Cu_{45}$ alloy is shown in Fig. 4.27. Similar dependences were observed for the $Pd_{70}Ag_{30}$-H and $Pd_{84}Au_{16}$-H solutions, the only difference being in the optimum hydrogen concentration for which the maximum value of T_c was observed ($n_{opt} \approx 0.7$, 0.8, and 0.9 respectively for the alloys with Cu, Ag, and Au).

The investigation of the $Pd_{60}Cu_{40}$ and $Pd_{80}Ag_{20}$ alloys (the compositions are close to optimum for obtaining the maximum T_c values for hydrogen implantation), saturated with hydrogen at $P_{H_2} \leqslant 7$ GPa, showed [4.97] that the $Pd_{60}Cu_{40}$-H solutions for $n \leqslant 0.6$ and at $T \geqslant 2$ K are not superconducting, while the T_c vs. n dependence for the $Pd_{80}Ag_{20}$-H solutions at $n \leqslant 1$ is close to that for the Pd-H solutions (see Fig. 4.27). The T_k vs. n dependences for the γ-solutions $Pd_{97}Au_3$-H, $Pd_{91}Au_9$-H [4.98], and $Pd_{90}Cu_{10}$-H (see Fig. 4.28), saturated with hydrogen at $P_{H_2} \leqslant 8$ GPa, were found to be approximately the same as for the Pd-H and $Pd_{80}Ag_{20}$-H solutions as well, which also disagrees with the data of [4.96].

Thus, our results show that the anomalously high values of T_c obtained with hydrogen implantation in alloys of palladium with noble metals are due to the peculiarities of metastable states arising upon implantation. It should be noted that at present there is no unified point of view as to how the alloying of palladium with noble metals should affect the superconducting transition tempera-

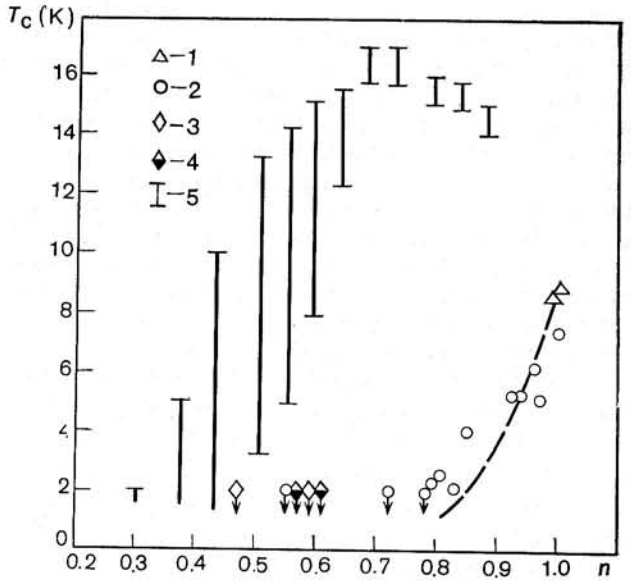

Fig. 4.27. Dependence of the superconducting transition temperature T_c on the hydrogen concentration n.
1—for the Pd-H solutions (results of the present paper); *2*—for γ-solutions $Pd_{80}Ag_{20}$-H [4.97]; *3*—for γ-solutions $Pd_{60}Cu_{40}$-H (results of the present paper); *4*—for γ′-solutions $Pd_{60}Cu_{40}$-H solutions [4.97] (symbols with arrows show that the samples are not superconducting at $T \geqslant 2$ K); *5*—for $Pd_{55}Cu_{45}$-H solutions [4.96] (the intervals in which the sample resistance changes from 90 to 10% of the value of residual resistance of the normal phase have been indicated). The dotted line shows the T_c vs. n dependence for the Pd-H solutions [4.51].

ture. For example, according to the theoretical estimates in [4.74, 99], this alloying should increase T_c, while the theoretical data in [4.100] and the estimates made in [4.101] on the basis of the experimental investigation of the low-temperature specific heat of nonsuperconducting $Pd_{80}Ag_{20}$-H solid solutions indicate that this temperature should decrease. The possibility that the instability of the crystal lattice (due to a softening of some phonon modes and a corresponding increase in the electron-phonon interaction constant) can play an important role in obtaining high T_c upon hydrogen implantation in palladium alloys with Cu, Ag, and Au was noted by Stritzker [4.96, 51] who discovered an interesting feature in the dependence of their T_c on the dose ψ of implanted hydrogen. For the Pd-Cu and Pd-Ag alloys with compositions close to optimum ($T_k^m \gtrsim 15$ K), the monotonic rise in T_c with increasing ψ was sometimes replaced by its sudden fall and vanishing of superconductivity for $T \geqslant 1$ K, while the residual resistance R_{res} decreased discontinuously by 10-20%. Further increase in ψ led to a monotonic decrease in R_{res}, but the appearance of superconductivity for $T \geqslant 1$ K was no longer observed. Stritzker explained this by the formation of a new nonsuperconducting phase with a smaller value of R_{res}.

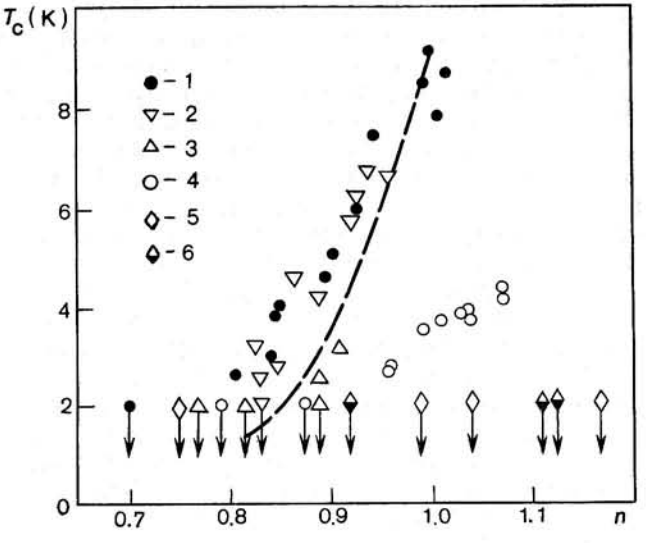

Fig. 4.28. T_c vs. n dependence for γ-solutions of hydrogen in the alloys.
1—$Pd_{90}Cu_{10}$ (results of the present paper); *2*, *3*—$Pd_{97}Au_3$ and $Pd_{91}Au_9$ [4.98]; *4*, *5*—$Pd_{95}Ni_5$ and $Pd_{80}Ni_{20}$ [4.110]; *6*—results for $Pd_{80}Ni_{20}$-H solutions consisting of a mixture of palladium-enriched and depleted phases. The arrows at the symbols and the dashed lines are the same as in Fig. 4.27.

The above discussion suggests that the appearance of superconductivity with anomalously high values of T_c accompanying implantation of hydrogen into palladium alloys with noble metals may be closely related just to the structural peculiarities of these systems. So, although according to the data available in the literature only ordinary γ-solutions of hydrogen on the basis of disordered metal lattice must be formed in the Pd-Cu-H [4.102], Pd-Ag-H [4.103, 104], and Pd-Au-H [4.105, 106] systems, we considered it expedient to carry out a structural analysis of such solutions. It turned out that under high hydrogen pressures, the Pd-Me-H systems may actually undergo new phase transformations which were never observed earlier upon hydrogenation of alloys of group VI-VIII transition metals and which are followed by a diffusion rearrangement of the atoms of the metallic matrix.

$Pd_{60}Cu_{40}$-H system [4.107]. The study of the isobars of the electrical resistance for the $Pd_{60}Cu_{40}$ alloy in a hydrogen atmosphere and

in the pressure interval of 0.5-2 GPa showed that an irreversible phase transition occurs in the samples upon heating above $T^* \approx \approx 200°C$, the resistance of the samples sharply decreasing during the phase transition. The transition proceeds quite slowly: even at 350° C, the drift in the resistance continues for tens of hours. X-ray studies revealed that the metallic sublattice of the $Pd_{60}Cu_{40}$-H samples obtained by exposing at $T = 200°C < T^*$ under hydrogen pressure $0.5 \leqslant P_{H_2} \leqslant 2$ GPa and having the composition $n \leqslant 0.47$ retains fcc symmetry and, in addition, the value of ΔV_0 of the jump in the unit cell volume of the $Pd_{60}Cu_{40}$ alloy accompanying hydrogenation agrees satisfactorily with the ΔV_0 vs. n dependence presented in [4.59] (see Fig. 4.16) for γ-solutions of hydrogen in palladium and its alloys. The $Pd_{60}Cu_{40}$-H samples obtained by exposing at $250 \leqslant T \leqslant 350°C$ (i.e. at $T > T^*$) had a metallic sublattice whose symmetry can be described on the basis of an fct (face-centered tetragonal) pseudocell (hereafter called the γ'-phase) with the axial ratio $0.94 \leqslant c/a \leqslant 0.97$. The hydrogen concentration in these specimens lay in the range $0.3 \leqslant n \leqslant 0.5$, and the volume per metal atom was nearly the same as for γ-solutions $Pd_{60}Cu_{40}$-H with similar values of n.

Further investigations revealed that the tetragonal structure of $Pd_{60}Cu_{40}$ alloys was retained even after quenching of γ'-samples in vacuum at 300° C, which led to *complete* liberation of hydrogen from the samples. The volume per metal atom decreased in this case to values close to those for the initial $Pd_{60}Cu_{40}$ alloy, while the tetragonality of the lattice grew. After quenching at $T \geqslant 350°$ C, the structure of the alloy returned to the starting fcc one. The return to the fcc structure occurred also after plastic deformation of the sample at room temperature. These results show that at atmospheric pressure and $T \geqslant 20°$ C, the γ'-structure of the $Pd_{60}Cu_{40}$ alloys is not a thermodynamically equilibrium one. At the same time, the metastability of this structure after complete evolution of hydrogen and even a certain increase in its degree of tetragonality support the proposition that the observed tetragonal distortions are mainly related not to the possible phase transformation in the hydrogen sublattice (for example, its ordering), but rather to a restructuring of the metal sublattice itself in the $Pd_{60}Cu_{40}$-H solution.

One of the possibilities of such restructuring is atomic ordering. The presence of wide regions with ordered atomic positioning in T vs. c diagrams is characteristic of the Cu-Pd system as well as a number of related systems. In particular, ordering in the region of compositions close to Cu_3Pd leads precisely to tetragonal distortion of the fcc lattice of Cu-Pd alloys [4.108, 109]. With ordering of this type, in addition to the main (structural) lines of the fct lattice, superstructural lines appear whose position is close to that for reflections from planes with mixed indices. For γ'-samples, in addition to the main lines, 11 weak and broad lines were observed, and mixed indices could be attributed to all of them.

Thus, the results of investigations [4.107] allows us to assert with quite a high degree of reliability that the formation of the γ'-phase in the $Pd_{60}Cu_{40}$-H system is accompanied by ordering of the metallic sublattice (although an incomplete one, which is indicated by the large width of the superstructural lines compared to that of the main lines). As regards the superconducting properties of $Pd_{60}Cu_{40}$-H solutions, it is hard to estimate at present the role of the instability of solutions with respect to ordering in obtaining anomalously high values of T_c reported in [4.96], since the structural investigations cannot be carried out for the samples saturated with hydrogen through implantation. If hydrogenation of the samples is performed under high pressures, superconductivity is absent at $T \geqslant 2$ K in both the γ- and γ'-solutions $Pd_{60}Cu_{40}$-H with $n \leqslant 0.6$ (see Fig. 4.27).

Pd-Ag-H system. We studied solutions formed on the basis of the alloys with 20, 50, and 78 at.% Ag at hydrogen pressures up to 6.7 GPa and temperatures up to 400° C. The $Pd_{50}Ag_{50}$-H system was found to be most interesting. At $P_{H_2} = 6.7$ GPa, phenomena completely analogous to those occurring in the $Pd_{60}Cu_{40}$-H system were observed for this system. At $T = 200°$ C, the system underwent an irreversible phase transition accompanied by a decrease in the sample resistance and a tetragonal distortion of its metal lattice. Tetragonality of the sample lattice was retained after complete liberation of hydrogen from the samples by quenching at $T \approx 250°$ C and disappeared after quenching at $T \geqslant 375°$ C or a plastic deformation of the samples without hydrogen at room temperature. The γ'-solutions $Pd_{50}Ag_{50}$-H differ from $Pd_{60}Cu_{40}$-H only in that the lattice of the former has $c/a < 1$. From the analogy between the properties of the Pd-Ag-H and Pd-Cu-H systems, it is reasonable to conclude that as in the $Pd_{60}Cu_{40}$-H system, the new phase transition observed in the $Pd_{50}Ag_{50}$-H system is accompanied by ordering of the metallic matrix (although superstructural lines were not observed in the X-ray photographs for the ordered $Pd_{50}Ag_{50}$-H solutions due to the nearly equal atomic scattering factors for palladium and silver).

On the basis of the data of resistometric and structural study of the samples obtained at high hydrogen pressures (see Table 4.3), the T vs. P_{H_2} phase diagram was constructed for the $Pd_{50}Ag_{50}$-H system (Fig. 4.29). Besides the lower limit of the temperature interval for the formation of the ordered γ'-phase (whose position is apparently determined by the kinetics of the process), the phase diagram also shows the line of the $\gamma' \rightleftarrows \gamma$ transformation which is the upper boundary of the temperature range for the thermodynamical stability of the γ'-solutions. Note that in the investigated range

Table 4.3. Data of X-ray Investigations at Atmospheric Pressure and $T = -190°$ C for $Pd_{50}Ag_{50}$-H Samples Obtained by Exposing for 24 Hours at T and P_{H_2} Indicated in Fig. 4.29

No.	n	a, Å	c, Å	c/a	ΔV_0, Å^3
1	0.38	4.042	—	—	3.7
2	0.52	3.995	4.249	1.064	5.5
3	0.50	3.985	4.259	1.069	5.3
4	0.48	3.986	4.271	1.073	5.5
5	0.51	3.985	4.283	1.075	5.7
6	0.44	4.062	—	—	4.7
7	0.44	3.987	4.242	1.064	5.1
8	0.44	3.991	4.228	1.059	5.0
9	0.43	3.996	4.217	1.055	5.0
10	0.43	3.989	4.224	1.059	4.9
11	0.44	4.007	4.193	1.046	5.0
12	0.39	4.049	—	—	4.1
13	0.29	4.043	—	—	3.8

Remark: We draw the reader's attention to the fact that the magnitudes of parameters for the γ'-solutions $Pd_{50}Ag_{50}$-H listed in the table are not the thermodynamically equilibrium values for given T and P_{H_2}, since a 24-hours exposure was obviously insufficient to bring the samples to the equilibrium state.

of hydrogen pressures, the temperature T_0 corresponding to disordering of the $Pd_{50}Ag_{50}$-H solutions was found to be much lower than that for the $Pd_{60}Cu_{40}$-H solutions for which $T_0 \gg 350°$ C at $0.5 \leqslant P_{H_2} \leqslant 2$ GPa [4.107].

As to the $Pd_{80}Ag_{20}$-H system, only ordinary γ-solutions based on disordered fcc metal lattice are formed in it at $P_{H_2} \leqslant 6.7$ GPa and $T \leqslant 400°$ C. According to the data of X-ray analysis, the $Pd_{22}Ag_{78}$-H solutions ($n \leqslant 0.09$) also have an fcc metal lattice.

The T_c vs. n dependence for the $Pd_{80}Ag_{20}$-H solutions is shown in Fig. 4.27. The investigated $Pd_{50}Ag_{50}$-H and $Pd_{22}Ag_{78}$-H solutions were not found to be superconducting for $T \geqslant 2$ K.

Pd-Au-H system. Investigations of hydrogen solutions in the alloys with 3, 9, 22.5, 50, and 75 at.% Au showed that at $P_{H_2} \leqslant 6.7$ GPa and $200 \leqslant T \leqslant 350°$ C, only ordinary γ-solutions on the basis of disordered lattice of the alloys are formed in the Pd-Au-H system [4.98]. Thus, if γ'-solutions are formed in the Pd-Au-H system at all, their disordering temperatures is below 200° C.

The dependence of the superconducting transition temperature on hydrogen concentration in the $Pd_{97}Au_3$ and $Pd_{91}Au_9$ alloys is

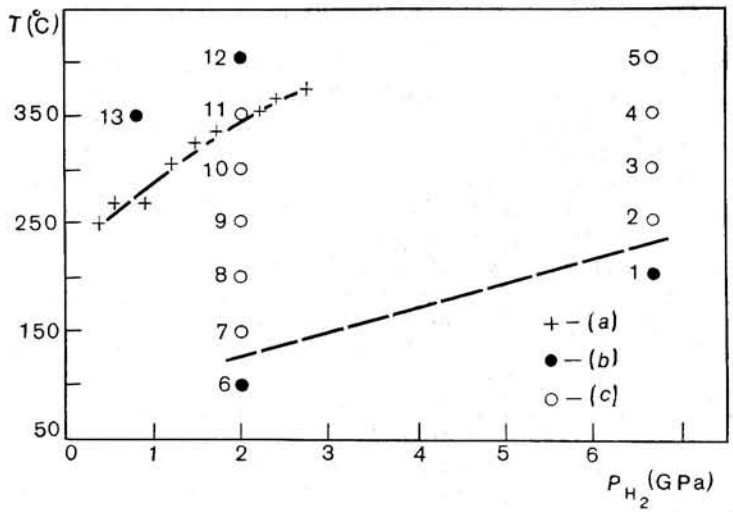

Fig. 4.29. T vs. P_{H_2} phase diagram for the $Pd_{50}Ag_{50}$-H system (results of the present paper).
a—values of the $\gamma' \rightleftarrows \gamma$ transition temperature. The dotted line is the lower limit of the temperature range in which the γ'-phase is formed. The numbers *1* to *13* indicate the conditions for obtaining the $Pd_{50}Ag_{50}$-H samples for investigations at normal pressure; data are shown in Table 4.3 (*b*—γ-solutions, *c*—γ'-solutions).

shown in Fig. 4.29. No superconducting transition was observed at $T \geqslant 2$ K for hydrogen solutions in alloys containing $\geqslant$22.5 at.% Au (the maximum hydrogen concentration attained for the alloys with 22.5, 50, and 75 at.% Au was $n = 0.61$, 0.25, and 0.03 respectively).

Pd-Ni-H system [4.110]. The alloys with 5, 20, 40, 60, and 80 at.% Ni were investigated. The measurements showed that at $P_{H_2} \leqslant 7$ GPa and $T \leqslant 250°$ C, only ordinary γ-solutions are formed in the Pd-Ni-H system, the line of the isomorphic $\gamma_1 \rightleftarrows \gamma_2$ transformation shifting monotonically towards higher pressures with increasing nickel content of the alloys. At $T > 250°$ C, the γ_2-solutions based on the alloys with 20, 40, 60, and 80 at.% Ni dissolute into hydrides of almost pure nickel and of palladium with a few atomic percent of Ni. The two-phase state of such samples is retained even after complete removal of hydrogen by annealing in vacuum at $T \leqslant 350°$ C. Quenching in vacuum at $T \geqslant 400°$ C or plastic deformation of hydrogen-free samples at room temperature returns the alloys to the starting homogeneous state. Hence, separation into phases enriched and depleted in palladium is not an equilibrium property of Pd-Ni solutions themselves under normal conditions.

It is the triple Pd-Ni-H solutions with a high hydrogen concentration which are found to dissolute.

Substitution of nickel for palladium leads to a suppression of superconductivity in the γ-solutions Pd-Ni-H (see Fig. 4.28), and γ-solutions based on the alloys with ⩾20 at. % Ni are not superconducting for $T \geqslant 2$ K [4.110]. Actually, it is just the behaviour of the superconducting properties that one should expect during alloying with a ferromagnetic metal. An unexpected result was the absence of superconductivity at $T \geqslant 2$ K for solutions based on the alloys with ⩾20 at. % Ni, dissoluted into palladium-enriched and depleted phases. This effect might be due to the suppression of superconductivity in particles of the palladium-enriched phase, precipitated from the Pd-Ni-H solid solution under the influence of the surrounding paramagnetic medium (the dimensions of the particles did not, in any case, exceed 0.5 μm). It is worth noting here that while the data on the superconductivity of Pd-Ni-H solutions obtained in samples saturated with hydrogen through implantation at helium temperature [4.51] and through electrolysis at $T \approx 200$ K [4.111] were in accord with our data [4.110], the hydrogenation of Pd-Ni alloys at a high hydrogen pressure and room temperature [4.112] led to different results: most of the samples based on alloys with ~20 and even 43 at. % Ni had rather high values of T_c. Crystal structure of the samples was not investigated in [4.112], but it is quite possible that samples with ⩾20 at. % Ni might consist of a mixture of palladium-enriched and depleted phases, and the palladium-enriched phase was superconducting.

Pd-Pt-H-system. The study of samples based on the alloys with 2.8, 10, 15, 20, 25, 40, and 60 at. % Pt showed that only ordinary γ-solutions are formed in the Pd-Pt-H system at $P_{H_2} \leqslant 6.5$ GPa and $T < 250°$ C, the solubility of hydrogen in the Pd-Pt alloys decreasing monotonically with increasing platinum concentration. At $T \geqslant 250°$ C, solutions based on the alloys containing ⩾15 at. % Pt dissolute into the hydride of palladium with a few atomic percent of Pt and the alloy with composition close to $Pd_{25}Pt_{75}$ in which hydrogen solubility at $P_{H_2} \leqslant 6.5$ GPa is negligible. After removal of the hydrogen through quenching in vacuum at 300° C, all the Pd-Pt samples return to their initial homogeneous state.

Figure 4.30 shows the data on the superconductivity of the Pd-Pt-H samples. The change in the T_c vs. n dependence for the γ-solutions with increasing platinum concentration in the alloys turned out to be nonmonotonic. The T_c vs. n dependence for the $Pd_{97.2}Pt_{2.8}$-H solutions is more gently sloping than that for the Pd-H solutions, and though at low values of n, the $Pd_{97.2}Pt_{2.8}$-H solutions possess higher values of T_c, the maximum T_c value reached for these solutions is lower than that for Pd-H. At $T \geqslant 2$ K, no superconductivity was observed for the $Pd_{90}Pt_{10}$-H solutions with

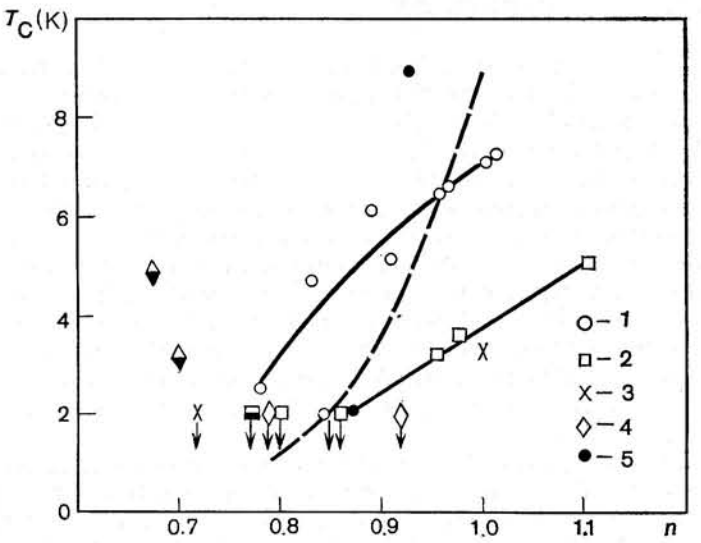

Fig. 4.30. Dependence of the superconducting transition temperature T_c on the hydrogen concentration n in Pd-Pt alloy containing: *1*—2.8; *2*—15; *3*—20; *4*—25 at. % Pt (results of the present paper); *5*—2.8 at. % Pt (results of [4.113]). Half-blackened symbols refer to the samples in which a separation into palladium-enriched and depleted phases are observed. The arrows and the dashed line are as in Fig. 4.27.

$n \leqslant 0.97$. Superconductivity reappeared in the $Pd_{85}Pt_{15}$-H and $Pd_{80}Pt_{20}$-H solutions, then vanished again, and the $Pd_{75}Pt_{25}$-H, $Pd_{60}Pt_{40}$-H, and $Pd_{40}Pt_{60}$-H solutions turned out to be nonsuperconducting at hydrogen concentrations up to $n = 0.92$, 0.51, and 0.11 respectively. In general, it should be remarked that the superconducting properties of the Pd-Pt-H system are found to be quite astonishing: our results on the behaviour of T_c differ from the results of [4.51] for the samples with implanted hydrogen (according to [4.51], $T_c^m \approx 9.5$ K for the alloys containing ⩽30 at. % Pt, and then decreases rapidly), as well as from the data of [4.113] for the $Pd_{97.2}Pt_{2.8}$ alloys saturated with hydrogen at high pressure and room temperature (see Fig. 4.30).

A gratifying result was the discovery of superconductivity in the two-phase $Pd_{75}Pt_{25}$-H samples (half-blackened diamond-shaped symbols in Fig. 4.30), which is in line with the inference that the Pd-Pt-H solutions dissolute into palladium-enriched and depleted phases at high hydrogen pressure and $T \geqslant 250°$ C.

It is the triple Pd-Ni-H solutions with a high hydrogen concentration which are found to dissolute.

Substitution of nickel for palladium leads to a suppression of superconductivity in the γ-solutions Pd-Ni-H (see Fig. 4.28), and γ-solutions based on the alloys with ⩾20 at. % Ni are not superconducting for $T \geqslant 2$ K [4.110]. Actually, it is just the behaviour of the superconducting properties that one should expect during alloying with a ferromagnetic metal. An unexpected result was the absence of superconductivity at $T \geqslant 2$ K for solutions based on the alloys with ⩾20 at. % Ni, dissoluted into palladium-enriched and depleted phases. This effect might be due to the suppression of superconductivity in particles of the palladium-enriched phase, precipitated from the Pd-Ni-H solid solution under the influence of the surrounding paramagnetic medium (the dimensions of the particles did not, in any case, exceed 0.5 μm). It is worth noting here that while the data on the superconductivity of Pd-Ni-H solutions obtained in samples saturated with hydrogen through implantation at helium temperature [4.51] and through electrolysis at $T \approx 200$ K [4.111] were in accord with our data [4.110], the hydrogenation of Pd-Ni alloys at a high hydrogen pressure and room temperature [4.112] led to different results: most of the samples based on alloys with ~20 and even 43 at. % Ni had rather high values of T_c. Crystal structure of the samples was not investigated in [4.112], but it is quite possible that samples with ⩾20 at. % Ni might consist of a mixture of palladium-enriched and depleted phases, and the palladium-enriched phase was superconducting.

Pd-Pt-H-system. The study of samples based on the alloys with 2.8, 10, 15, 20, 25, 40, and 60 at. % Pt showed that only ordinary γ-solutions are formed in the Pd-Pt-H system at $P_{H_2} \leqslant 6.5$ GPa and $T < 250°$ C, the solubility of hydrogen in the Pd-Pt alloys decreasing monotonically with increasing platinum concentration. At $T \geqslant 250°$ C, solutions based on the alloys containing ⩾15 at. % Pt dissolute into the hydride of palladium with a few atomic percent of Pt and the alloy with composition close to $Pd_{25}Pt_{75}$ in which hydrogen solubility at $P_{H_2} \leqslant 6.5$ GPa is negligible. After removal of the hydrogen through quenching in vacuum at 300° C, all the Pd-Pt samples return to their initial homogeneous state.

Figure 4.30 shows the data on the superconductivity of the Pd-Pt-H samples. The change in the T_c vs. n dependence for the γ-solutions with increasing platinum concentration in the alloys turned out to be nonmonotonic. The T_c vs. n dependence for the $Pd_{97.2}Pt_{2.8}$-H solutions is more gently sloping than that for the Pd-H solutions, and though at low values of n, the $Pd_{97.2}Pt_{2.8}$-H solutions possess higher values of T_c, the maximum T_c value reached for these solutions is lower than that for Pd-H. At $T \geqslant 2$ K, no superconductivity was observed for the $Pd_{90}Pt_{10}$-H solutions with

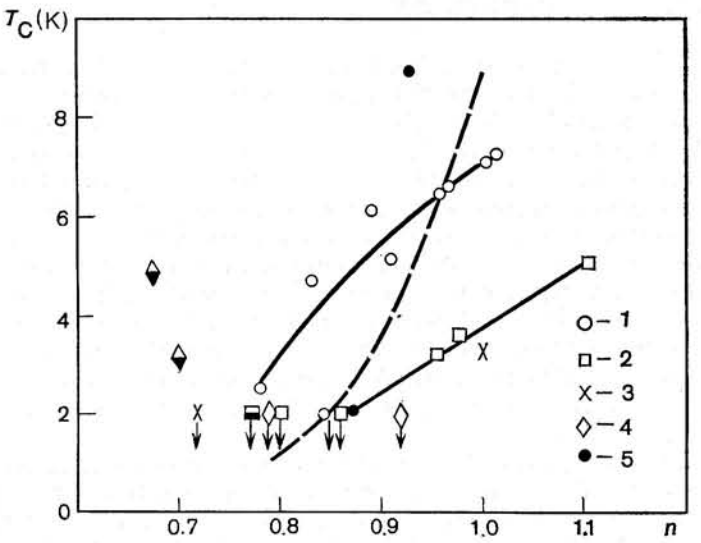

Fig. 4.30. Dependence of the superconducting transition temperature T_c on the hydrogen concentration n in Pd-Pt alloy containing: *1*—2.8; *2*—15; *3*—20; *4*—25 at. % Pt (results of the present paper); *5*—2.8 at. % Pt (results of [4.113]). Half-blackened symbols refer to the samples in which a separation into palladium-enriched and depleted phases are observed. The arrows and the dashed line are as in Fig. 4.27.

$n \leqslant 0.97$. Superconductivity reappeared in the $Pd_{85}Pt_{15}$-H and $Pd_{80}Pt_{20}$-H solutions, then vanished again, and the $Pd_{75}Pt_{25}$-H, $Pd_{60}Pt_{40}$-H, and $Pd_{40}Pt_{60}$-H solutions turned out to be nonsuperconducting at hydrogen concentrations up to $n = 0.92$, 0.51, and 0.11 respectively. In general, it should be remarked that the superconducting properties of the Pd-Pt-H system are found to be quite astonishing: our results on the behaviour of T_c differ from the results of [4.51] for the samples with implanted hydrogen (according to [4.51], $T_c^m \approx 9.5$ K for the alloys containing ⩽30 at. % Pt, and then decreases rapidly), as well as from the data of [4.113] for the $Pd_{97.2}Pt_{2.8}$ alloys saturated with hydrogen at high pressure and room temperature (see Fig. 4.30).

A gratifying result was the discovery of superconductivity in the two-phase $Pd_{75}Pt_{25}$-H samples (half-blackened diamond-shaped symbols in Fig. 4.30), which is in line with the inference that the Pd-Pt-H solutions dissolute into palladium-enriched and depleted phases at high hydrogen pressure and $T \geqslant 250°$ C.

4.6. CONCLUSION

As is seen from the results described in this paper, the technique for compressing hydrogen to high pressures turned out to be quite a valuable tool for investigating the metal-hydrogen systems. With the help of this technique, over a relatively short period of time, hydrides were obtained for most of the group VI-VIII transition metals which were earlier considered to form no hydrogen-saturated phases. The crystal structure and composition of these new hydrides were studied and the diagrams of phase transformations were constructed. It seems now that there are no transition metals which do not form hydrides at all, and one can expect that a further extension of the pressure range will result in the injection of considerable amounts of hydrogen even in metals like tungsten, osmium, iridium, and platinum, the most inert metals with respect to hydrogen.

The possibility of varying the hydrogen concentration in 3*d*-metals of VI-VIII groups over a wide range led to a lot of new experimental results which helped in constructing a systematic picture of the effect of hydrogen on the magnetic properties of transition metals. An analysis of the accumulated experimental data shows that all the observed effects stem primarily from the increase in the degree of filling of the weakly deforming *d*-band of the metal-solvent by electrons, the hydrogen supplying a fractional number of electrons ($\eta < 1$ electron per proton) to the *d*-band (the rigid *d*-band model). It is worth mentioning that the concept of the hydrogen as a donor of a fractional number of electrons to the *d*-band of the metal-solvent agrees with the theoretical calculations carried out by other authors on the band structure of the hydrides of transition metals.

The study of the Pd-Me-H solutions showed that homogeneous thick samples saturated with hydrogen under pressure and in near-equilibrium conditions do not reveal anomalous superconducting properties which were earlier observed in the experiments on hydrogen implantation. Therefore, the unusual behaviour of T_c for the Pd-Me-H solutions obtained by implantation is not a property of the equilibrium solutions but is due to the peculiarities of the metastable state of thin and defect-saturated hydrogen-containing layers formed in the process of implantation. The fact that the Pd-Me-H solutions obtained by implantation possess considerably higher values of T_c as compared to those for the equilibrium solutions throws a new light on the possibilities of improving the superconducting properties by using various metastable states of a material, including an adjustment of its defect structure.

An interesting result of our investigations of the Pd-Me-H systems is the discovery of new phase transformations accompanied by a diffusion rearrangement of atoms of the metal matrix and occurring at comparatively low temperature. The discovery of such transformations is yet another convincing proof of the extremely strong influence of hydrogen on the interatomic interaction and diffusion mobility of the metallic components of the hydrogenated alloys.

Thus, the new experimental results obtained with the help of the high pressure technique have significantly contributed toward clarifying the important problems concerning the physical status of hydrogen in transition metals and the processes that can occur when the alloys of transition metals interact with hydrogen in the state of enhanced activity, i.e. with hydrogen compressed to high static and dynamic pressures, hydrogen in strong electrolytes, and hydrogen plasma.

References

4.1. V. Kh. Alimov, A. E. Gorodetsky, A. P. Zakharov, V. M. Sharapov, *Dokl. Akad. Nauk SSSR*, **241**, 595 (1978).
4.2. B. Stritzker, *Phys. Rev. Lett.*, **42**, 1769 (1979).
4.3. B. Baranowski, R. Wiśniewski, *Bull. Akad. Polon. Sci.*, **14**, 273 (1966); R. Wiśniewski. In: *III Krajowa Narada Techniki Wysokich Ciśnień*, Warszawa, 1969; B. Baranowski, W. Bujnowski, *Roczn. Chem.*, **44**, 2271 (1970).
4.4. B. Baranowski, *Ber. Bunsenges. phys. Chem.*, **76**, 714 (1972).
4.5. B. Baranowski, *Topics in Appl. Phys.*, **29**, 157 (1978).
4.6. B. Baranowski, *Z. phys. Chem.* N. F., **114**, 59 (1979).
4.7. I. T. Belash, E. G. Ponyatovsky, Patent No. 741105 (USSR).
4.8. V. E. Antonov, I. T. Belash, E. G. Ponyatovsky. In: *Fizika i Tekhnika Vysokikh Davleny*, 9, 65 (1982), Naukova Dumka, Kiev; *Proc. 8th AIRAPT/19th EHPRG Conf.* 1, 80 (1981), Uppsala, Sweden.
4.9. V. E. Antonov, T. E. Antonova, I. T. Belash, A. E. Gorodetsky, E. G. Ponyatovsky, *Dokl. Akad. Nauk SSSR*, **266**, 376 (1982).
4.10. S. A. Semiletov, R. V. Baranova, Yu. P. Khodyrev, R. M. Imamov, *Kristallografiya*, **25**, 1162 (1980).
4.11. E. Wicke, H. Brodowsky, *Topics in Appl. Phys.*, **29**, 73 (1978).
4.12. V. E. Antonov, I. T. Belash, E. G. Ponyatovsky, V. I. Rashupkin, *Fiz. Metallov i Metallovedenie*, 48, 75 (1979).
4.13. V. E. Antonov, I. T. Belash, E. G. Ponyatovsky, *Dokl. Akad. Nauk SSSR*, **223**, 1114 (1977).
4.14. V. I. Spitsyn, V. E. Antonov, O. A. Balakhovsky, I. T. Belash, E. G. Ponyatovsky, V. I. Rashupkin, V. Sh. Shekhtman, *Dokl. Akad. Nauk SSSR*, **260**, 132 (1981).
4.15. M. Krukowski, B. Baranowski, *Roczn. Chem.*, 49, 1183 (1975).
4.16. E. G. Ponyatovsky, I. T. Belash, *Dokl. Akad. Nauk SSSR*, **224**, 607 (1975).
4.17. V. I. Spitsyn, E. G. Ponyatovsky, V. E. Antonov, I. T. Belash, O. A. Balakhovsky, *Dokl. Akad. Nauk SSSR*, **247**, 1420 (1979).
4.18. V. E. Antonov, I. T. Belash, V. F. Degtyareva, E. G. Ponyatovsky, V. I. Shiryaev, *Dokl. Akad. Nauk SSSR*, **252**, 1384 (1980).
4.19. V. E. Antonov, I. T. Belash, V. F. Degtyareva, E. G. Ponyatovsky, *Dokl. Akad. Nauk SSSR*, **239**, 342 (1978).
4.20. A. Knödler, Metaloberfl, **17**, 161 (1963); A. D. Stock, K. I. Hardcastle, *J. Inorg. Nucl. Chem.*, **32**, 1183 (1970); G. Wolf, *Z. phys. Chem.* (Leipzig), **246**, 403 (1971); H. R. Khan *et al.*, *Math. Res. Bull.*, 9, 1191 (1974).

4.21. B. Baranowski, K. Bojarski, *Roczn. Chem.*, **46**, 525 (1972).
4.22. E. G. Ponyatovsky, I. T. Belash, *Dokl. Akad. Nauk SSSR*, **229**, 1171 (1976).
4.23. B. Baranowski, K. Bojarski, *Roszn. Chem.*, 46, 1403 (1972).
4.24. I. T. Belash, V. E. Antonov, E. G. Ponyatovsky, *Dokl. Akad. Nauk SSSR*, **235**, 379 (1977).
4.25. V. E. Antonov, I. T. Belash, E. G. Ponyatovsky, *Dokl. Akad. Nauk SSSR*, **248**, 635 (1979).
4.26. M. Krukowski, B. Baranowski, *J. Less-Common Metals*, 49, 385 (1976).
4.27. I. T. Belash, B. K. Ponomarev, V. G. Thiessen, N. S. Afonikova, V. Sh. Shekhtman, E. G. Ponyatovsky, *Fiz. Tverd. Tela*, **20**, 422 (1978).
4.28. V. P. Zhebelev, V. A. Somenkov, E. G. Ponyatovsky, S. Sh. Shilshtein, I. T. Belash, *Neorgan. Mater.*, **14**, 1620 (1978).
4.29. E. G. Ponyatovsky, V. E. Antonov, I. T. Belash, *Uspekhi Fiz. Nauk*, **137**, 663 (1982).
4.30. V. E. Antonov, I. T. Belash, V. Yu. Malyshev, E. G. Ponyatovsky, N. A. Tulina, *Dokl. Akad. Nauk SSSR*, **269**, 617 (1983).
4.31. V. E. Antonov, I. T. Belash, E. G. Ponyatovsky, *Scripta Metal.*, **16**, 203 (1982).
4.32. J. F. Cannon, *J. Phys. Chem. Ref. Data*, **3**, 781 (1974).
4.33. E. G. Ponyatovsky, V. E. Antonov, I. T. Belash, *Fiz. Metallov i Metallovedenie*, **44**, 1038 (1977); **46**, 1090 (1978).
4.34. E. G. Ponyatovsky, V. E. Antonov, I. T. Belash, *Fiz. Metallov i Metallovedenie*, **46**, 1090 (1978).
4.35. F. P. Bundy, *J. Appl. Phys.*, **36**, 616 (1965).
4.36. L. D. Blackburn, L. Kaufmann, M. Cohen, *Acta Metal.*, **13**, 533 (1965).
4.37. V. E. Antonov, I. T. Belash, E. G. Ponyatovsky, V. G. Thiessen, V. I. Shiryaev, *Phys. Stat. Sol.* (a), **65**, K43 (1981).
4.38. G. C. Kennedy, R. C. Newton, In: *Solids under Pressure*, N.Y.-London, 1963, p. 163-178.
4.39. I. T. Belash, V. E. Antonov, E. G. Ponyatovsky, *Dokl. Akad. Nauk SSSR*, **235**, 128 (1977).
4.40. V. E. Antonov, I. T. Belash, B. K. Ponomarev, E. G. Ponyatovsky, V. G. Thiessen, *Phys. Stat. Sol.* (a), **57**, 75 (1980).
4.41. B. Baranowski, M. Smiałowski, *J. Phys. Chem. Solids*, **12**, 206 (1959); *Bull. Acad. Polon. Sci.*, **7**, 663 (1958).
4.42. B. Baranowski, R. Wiśniewski, *Bull. Acad. Polon. Sci.*, **14**, 273 (1966).
4.43. E. G. Ponyatovsky, V. E. Antonov, I. T. Belash, *Dokl. Akad. Nauk SSSR*, **229**, 391 (1976).
4.44. E. G. Ponyatovsky, V. E. Antonov, I. T. Belash, *Dokl. Akad. Nauk SSSR*, **230**, 649 (1976).
4.45. V. G. Thiessen, V. E. Antonov, I. T. Belash, B. K. Ponomarev, E. G. Ponyatovsky, *Dokl. Akad. Nauk SSSR*, **242**, 1390 (1978).
4.46. D. Bloch, *Ann. de Phys.*, **1**, 3 (1966).
4.47. V. E. Antonov, I. T. Belash, V. M. Koltygin, E. G. Ponyatovsky, *Dokl. Akad. Nauk SSSR*, **248**, 131 (1979).
4.48. T. Graham, *Proc. Roy. Soc.*, **16**, 422 (1868); *Phil. Mag.*, **36**, 63 (1868); *C. R. Ac. Sci.*, **66**, 1014 (1868); *Ann. Chim. Phys.* (Paris), **14**, 315 (1868).
4.49. D. M. Nace, J. G. Aston, *J. Am. Soc.*, **79**, 3623, 3627 (1957).
4.50. T. Skośkiewicz, *Phys. Stat. Sol.* (a), **11**, K123 (1972).
4.51. B. Stritzker, H. Wühl, *Topics in Appl. Phys.*, **29**, 243 (1978).
4.52. M. Hansen, K. Anderko. *Constitution of Binary Alloys*, McGraw-Hill Book Company, N. Y./Toronto/London, 1958.
4.53. B. Baranowski, S. Filipek, *Roczn. Chem.*, **47**, 2165 (1973).
4.54. V. E. Antonov, I. T. Belash, V. F. Degtyareva, E. G. Ponyatovsky, V. G. Thiessen, *Fiz. Metallov i Metallovedenie*, **53**, 677 (1982).
4.55. B. Baranowski, M. Tkacz, *Europhys. Conf. Abstr.*, **1A**, 108, (1975).

4.56. V. E. Antonov, I. T. Belash, V. G. Thiessen, *Phys. Stat. Sol.* (a), **59**, 673 (1980).
4.57. M. Krukowski, B. Baranowski, *J. Less-Common Metals*, **49**, 385 (1976).
4.58. V. E. Antonov, I. T. Belash, V. F. Degtyareva, B. K. Ponomarev, E. G. Ponyatovsky, V. G. Thiessen, *Fiz. Tverd. Tela*, **20**, 2680 (1978).
4.59. B. Baranowski, S. Majchrzak, T. B. Flanagan, *J. Phys. F: Metal Phys.*, **1**, 258 (1971).
4.60. E. O. Wollan, J. W. Cable, W. C. Koehler, *J. Phys. Chem. Sol.*, **24**, 1141 (1963).
4.61. W. E. Wallace, *Ber Bunsenges. phys. Chem.*, **76**, 832 (1972).
4.62. M. Hanson, H. R. Khan, A. Knödler, Ch. J. Raub., *J. Less-Common Metals*, **43**, 93 (1975).
4.63. H. R. Khan, Ch. J. Raub, *J. Less-Common Metals*, **49**, 399 (1976).
4.64. V. G. Thiessen, V. E. Antonov, I. T. Belash, B. K. Ponomarev, E. G. Ponyatovsky, *Phys. Stat. Sol.* (a), **48**, K185 (1978).
4.65. J. Crangle, G. C. Hallam, *Proc. Roy. Soc.*, **272A**, 119 (1963).
4.66. S. V. Vonsovsky, *Magnetizm*, Nauka, Moskva, 1971 (in Russian).
4.67. M. J. Besnus, Y. Gottehrer, G. Munschy, *Phys. Stat. Sol.* (b), **49**, 597 (1972).
4.68. B. K. Ponomarev, V. G. Thiessen, *Zh. Eksper. Teor. Fiz.*, **73**, 332 (1977).
4.69. J. Friedel, *J. Phys. et Rad.*, **19**, 573 (1958); **23**, 692 (1962); *Nuovo Cimento Suppl.*, **7**, 287 (1958).
4.70. G. T. Dubovka, *Phys. Stat. Sol.*, (a), **24**, 375 (1974).
4.71. J. Friedel, *Ber. Bunsenges. phys. Chem.*, **76**, 828 (1972).
4.72. A. C. Switendick, *Sol. State Comm.*, 8, 1463 (1970); *Ber. Bunsenges. phys. Chem.*, **76**, 535 (1972); *Topics in Appl. Phys.*, **28**, 101 (1978).
4.73. D. A. Papaconstantopoulos, B. M. Klein, *Phys. Rev. Lett.*, **35**, 110 (1975); D. A. Papaconstantopoulos, B. M. Klein, J. S. Faulkner, L. L. Boyer, *Phys. Rev.*, **B18**, 2784 (1978).
4.74. D. A. Papaconstantopoulos, B. M. Klein, E. N. Economou, L. L. Boyer, *Phys. Rev.*, **B17**, 141 (1978); D. A. Papaconstantopoulos, E. N. Economou, B. M. Klein, L. L. Boyer. In: *Proc. Intern. Meeting on Hydrogen in Metals.* Münster, 1979, p. 733; *Phys. Rev.*, **B20**, 177 (1979).
4.75. M. Gupta, A. J. Freeman, *Phys. Rev.*, **B17**, 3029 (1978).
4.76. N. I. Kulikov, V. N. Borzunov, A. D. Zvonkov, *Phys. Stat. Sol.* (b), 86, 83 (1978).
4.77. J. M. Leger, C. Loriers-Susse, B. Vodar, *Phys. Rev.*, **B6**, 4250 (1972).
4.78. H. J. Schenk, H. J. Bauer. In: *Proc. Intern. Meeting on Hydrogen in Metals.* Münster, 1979, p. 350.
4.79. H. J. Schenk, H. J. Bauer, B. Baranowski, *Phys. Stat. Sol.* (a), **52**, 195 (1979).
4.80. G. J. Zimmermann, H. J. Bauer, *Z. Phys.*, **229**, 154 (1969).
4.81. B. K. Ponomarev, S. V. Alexandrovich, *Zh. Eksper. Teor. Fiz.*, **67**, 1965 (1974).
4.82. G. T. Dubovka, E. G. Ponyatovsky, I. Ya. Georgieva, V. E. Antonov, *Phys. Stat. Sol.* (a), **32**, 301 (1975).
4.83. V. E. Antonov, I. T. Belash, B. K. Ponomarev, E. G. Ponyatovsky, V. G. Thiessen, *Phys. Stat. Sol.* (a), **52**, 703 (1979).
4.84. T. Sohmura, F. E. Fujita, *Sol. State Comm.*, **25**, 43 (1978).
4.85. D. M. Edwards, E. P. Wohlfarth, *Proc. Roy. Soc.*, **303A**, 127 (1968); E. P. Wohlfarth, *J. Appl. Phys.*, **39**, 1061 (1968).
4.86. V. E. Antonov, G. T. Dubovka, *Fiz. Metallov i Metallovedenie*, **40**, 645 (1976).
4.87. E. G. Ponyatovsky, V. E. Antonov, I. T. Belash, *Fiz. Tverd. Tela*, **18**, 3661 (1976).
4.88. H. J. Bauer, G. Berninger, G. Zimmermann, *Z. Naturforsch.*, **23a**, 2023 (1968); H. J. Bauer, *Z. angew. Phys.*, **26**, 87 (1968).

4.89. V. E. Antonov, I. T. Belash, V. F. Degtyareva, E. G. Ponyatovsky, V. G. Thiessen, *Fiz. Metallov i Metallovedenie*, **53**, 677 (1982).
4.90. P. Weiss, R. Forrer, *Ann. de Phys.*, **12**, 279 (1929).
4.91. R. M. Bozorth, *Ferromagnetism*. D. van Nostrand, Toronto/New York/London, 1951.
4.92. H. Ohno, *J. Phys. Soc. Japan*, **31**, 92 (1971).
4.93. H. Ohno, M. Mekata, *J. Phys. Soc. Japan.*, **31**, 102 (1971).
4.94. V. E. Antonov, I. T. Belash, I. Ya. Georgieva, V. F. Degtyareva, V. G. Thiessen, A. V. Shalimova, *Fiz. Tverd. Tela*, **24**, 975 (1982).
4.95. E. Wicke, *J. Less-Common Metals*, **74**, 185 (1980).
4.96. B. Stritzker, *Z. Phys.*, **268**, 261 (1974).
4.97. V. E. Antonov, I. T. Belash, E. G. Ponyatovsky, V. I. Rashupkin, *Zh. Eksper. Teor. Fiz., Pis'ma*, **31**, 451 (1980).
4.98. V. E. Antonov, T. E. Antonova, I. T. Belash, E. G. Ponyatosky, V. I. Rashupkin, *Phys. Stat. Sol.* (a), **77**, K 23 (1983).
4.99. B. N. Ganguly, *Z. Phys.*, **B22**, 127 (1975).
4.100. K. H. Bennemann, J. W. Garland, *Z. Phys.*, **260**, 367 (1973).
4.101. G. Wolf, J. Yanke, K. Bohmhammel, *Phys. Stat. Sol.* (a), **36**, K125 (1976).
4.102. T. B. Flanagan, D. M. Chisdes, *Sol. State Comm.*, **16**, 529 (1975); D. Fisher, D.M. Chisdes, T. B. Flanagan, *J. Sol. State Chem.*, **20**, 149 (1977).
4.103. H. Brodowsky, E. Poeschel, *Z. Phys. Chem. N.F.*, **44**, 143 (1965).
4.104. A. W. Szafrański, B. Baranowski, *Phys. Stat. Sol.* (a), **9**, 435 (1972).
4.105. A. Maeland, T. B. Flanagan, *J. Phys. Chem.*, **69**, 3575 (1965).
4.106. B. Baranowski, R. Wiśniewski, *Phys. Stat. Sol.*, **35**, 593 (1969).
4.107. V. F. Degtyareva, V. E. Antonov, I. T. Belash, E. G. Ponyatovsky, *Phys. Stat. Sol.* (a), **66**, 77 (1981).
4.108. W. B. Pearson, *A Handbook of Lattice Spacings and Structures of Metals and Alloys*. Pergamon Press, London, 1964.
4.109. K. Schubert, B. Kiefer, M. Wilkens, R. Haufler, *Z. Metallkunde*, **46**, 692 (1955); D. M. Jones, E. A. Owen, *Proc. Phys. Soc.*, **67A**, 297 (1954).
4.110. V. E. Antonov, T. E. Antonova, I. T. Belash, E. G. Ponyatovsky, V. I. Rashupkin, V. G. Thiessen, *Phys. Stat. Sol.* (a), **77**, 71 (1983).
4.111. L. Sniadower, L. Dumoulin, P. Nedellec, J. P. Burger. In: *Metall-Hydrogen Systems*, Ed. T.N. Veziroğlu, Pergamon Press, Oxford, 1982.
4.112. T. Skośkiewicz, *High Temp.-High Pressures*, **7**, 684 (1975); *Phys. Stat. Sol.* (a), **48**, K165 (1978).
4.113. T. Skośkiewicz, A. W. Szafrański, B. Baranowski, *Phys. Stat. Sol.* (b), **59**, K135 (1973).
4.114. B. Baranowski, K. Bocheńska, *Roczn. Chem.*, 38, 1419 (1964); *Z. Phys. Chem. N.F.*, **45**, 140 (1965).
4.115. S. Majchrzak, *Bull. Acad. Polon. Sci.*, **15**, 485 (1967).

5 Dislocations and Physical Properties of Semiconductors

Yu. A. Ossipyan

5.1. INTRODUCTION

The main concepts about the influence of dislocations on the electric properties of semiconductors are based on the model in which a dislocation chain is treated as a line of atoms with dangling chemical bonds. These atoms may capture electrons from the conduction band or, conversely, give away unpaired electrons to other centres, thus acting as acceptors or donors. Consequently, the dislocations in semiconductors possess an electric charge. This leads to a sharp anisotropic change in the carrier mobility upon introduction of dislocations into a crystal. Investigations of the energy spectrum of electrons directly involved in dislocation states are also of considerable interest. It is found that these electrons account for such properties of plastically deformed semiconductors as dislocation electric conductivity and dislocation EPR.

All this indicates that the electron properties of semiconductors with dislocations are quite different from the properties of defect-free crystals.

However, the electron-dislocation interaction in semiconductors is not confined to just these properties. It has been experimentally shown that the state of the electron subsystem and its variation have a considerable effect on the movement of dislocations under the action of mechanical loads, i.e. on the strength and plasticity of semiconductors. This has been confirmed by the discovery of photoplastic effect, electroplastic effect, dislocation current and dislocation luminescence, and several other effects during the last few years. The essence of these phenomena lies in the fact that when an electron subsystem is excited by light or an electric field, the dislocation levels as well as the levels of other local centres are occupied nonuniformly by the electrons. Under these conditions, an excess electric charge is created on the dislocations, thus ensuring the hardening of the crystal. A moving dislocation sweeps the electrons from the local centres into the conduction band. It is the return of these electrons to lower energy states that causes dislocation luminescence.

In this review, we shall be considering both the above-mentioned aspects of the electron-dislocation interaction. We shall present